The Water Budget of the Kuparuk River Basin, Alaska*

STEPHEN J. DÉRY+

Lamont-Doherty Earth Observatory, Columbia University, Palisades, New York

MARC STIEGLITZ

School of Civil and Environmental Engineering and School of Earth and Atmospheric Sciences, Georgia Institute of Technology, Atlanta, Georgia

ÅSA K. RENNERMALM AND ERIC F. WOOD

Department of Civil and Environmental Engineering, Princeton University, Princeton, New Jersey

(Manuscript received 30 August 2004, in final form 11 February 2005)

ABSTRACT

A water budget study that considers precipitation, river runoff, evapotranspiration, and soil moisture for the Kuparuk River basin on the North Slope of Alaska is presented. Numerical simulations of hydrologic processes using the NASA Catchment-based Land Surface Model are conducted for the period 1991–2001 and provide the partitioning of the observed precipitation input (292 mm yr^{-1}) onto the basin into river discharge (169 mm yr^{-1}), evapotranspiration (127 mm yr^{-1}), and an increase in soil moisture (1 mm yr^{-1}). Discharge attains its annual peak during snowmelt and disposes 58% of the annual precipitation. Evapotranspiration contributes another 43% to the water budget and is mainly associated with warm summertime conditions and a snow-free surface. Combined, surface-snow and blowing-snow sublimation contribute only 5% of the total annual evaporative fluxes. Soil moisture recharge is associated with snowmelt during spring and rainfall during late summer and early fall, whereas soil drying accompanies high evapotranspiration rates during summer. An analysis of interannual variability in the water budget shows that warm, dry years favor a relatively more intense response of river discharge and evapotranspiration to the precipitation input, whereas cool, wet years tend to augment soil moisture.

1. Introduction

Over the past century, the Arctic has undergone regional warming at rates of 0.5°C or more per decade (Chapman and Walsh 1993). This has induced changes in other hydrometeorological conditions, including an increase in precipitation (e.g., Serreze et al. 2000; Walsh 2000), an intensification of freshwater discharge from major rivers (Peterson et al. 2002), and an enhancement of evapotranspiration fluxes (Serreze et al. 2003). As Arctic precipitation is augmenting, there remains uncertainty on how the additional input of freshwater will be partitioned on the land surface into streamflow and evapotranspiration. For instance, will one of these two processes become more important, or will their relative contribution (as a percentage of the precipitation input) remain stable in time? Will the interplay between these processes significantly alter soil moisture conditions? A modeling study by Hinzman and Kane (1992) suggests that rising air temperatures will sufficiently enhance the atmospheric demand for moisture so as to overwhelm any increase in precipitation. In turn, this would lead to a drying out of soils on the North Slope of Alaska. Barber et al. (2000) present evidence of this tendency in the boreal forest near Fairbanks, Alaska, where there has been a reduction in the growth

* Lamont-Doherty Earth Observatory Contribution Number 6734.

+ Current affiliation: Program in Atmospheric and Oceanic Sciences, Princeton University, Princeton, New Jersey.

Corresponding author address: Stephen J. Déry, Program in Atmospheric and Oceanic Sciences, Princeton University, 307 GFDL, Princeton, NJ 08542-0308.
E-mail: sdery@princeton.edu

© 2005 American Meteorological Society

of white spruce as a consequence of temperature-induced drought stress over the twentieth century. In a modeling study of carbon dynamics in Arctic tundra, Stieglitz et al. (2000) come to the conclusion that precipitation rates in a warmer environment will be sufficient to counter any increase in evaporative fluxes, thereby leading to wetter soil conditions and enhanced river runoff. This conclusion is in accordance with the observed trends in Siberian river discharge (Peterson et al. 2002).

This study is motivated by the uncertainties that remain in our understanding of the land surface's response to past and potential future changes in the atmospheric state. To better comprehend the role of climate change and climate variability on hydrologic processes of Arctic watersheds, a water budget study for the Kuparuk River basin (KRB) on the North Slope of Alaska in presented. A modeling approach is used, owing to the lack of comprehensive observations of soil moisture and evapotranspiration in the KRB. The goal of this study is to obtain a long-term climatology of water budget terms for the KRB and to explore the effects of climate variability on the partitioning of precipitation into evapotranspiration, river runoff, and changes in soil moisture in this watershed. This provides some important insights on the possible response of the Arctic land surface to a changing environment. Useful information on the processes that need to be resolved by land surface schemes to accurately simulate the water budget of Arctic watersheds is also presented.

2. The Kuparuk River basin

a. Physical setting and climate

The Kuparuk River basin is situated north of the Brooks Range and flows northward about 250 km into the Arctic Ocean (Fig. 1). This basin is centered near 70°N, 150°W and covers approximately 8421 km^2 in area on the North Slope of Alaska at an average altitude of 263 m above mean sea level (Table 1). The KRB spans three principal physiographic regions, beginning with the mountainous headwaters of the Brooks Range, then the Arctic foothills, and finally the flat Arctic Coastal Plain near the river's mouth at Prudhoe Bay. Organic peat composes the top 15–20-cm soil layer with mineral soils at greater depths (Hinzman et al. 1991, 1996). The basin is underlain by continuous permafrost that reaches depths as great as 600 m (Osterkamp and Payne 1981). The frozen ground acts as an impermeable boundary that hinders deep water infiltration (McNamara et al. 1998). During summer, thawing of the active layer remains shallow, reaching depths from 0.25 to 1.0 m (Hinzman et al. 1991; Zhang et al. 1997). The diminutive vegetation consists generally of tussock tundra, shrubs, wet sedge, dry heath, and lichens (Walker and Walker 1996).

The climate of the KRB is dominated by the lengthy cold season during which snow covers the surface for about two-thirds of the year. Snowmelt is between mid-May and mid-June and provides up to 80% of the river's annual runoff into the Arctic Ocean (McNamara et al. 1998). Total snowfall amounts are relatively light, with a typical value of 120-mm snow water equivalent (swe) in any given year. Yet, snowfall (swe) accounts for about half of the annual precipitation input into the catchment and may occur at any time of the year. The mean annual air temperature for the Kuparuk nears −10°C (Zhang et al. 1996). High-wind conditions and blowing-snow events are also common in the basin, especially near the Arctic coastline and in mountainous regions (Déry and Yau 1999; Liston and Sturm 2002).

Similar to other Arctic regions, the KRB has been the site of rapid climate change during the past few decades. Near-surface air temperatures have warmed by about 2°C over the past 20 yr (Chapman and Walsh 1993; Serreze et al. 2000). In response to the rising air temperatures and to recent increases in snow depth, significant warming in permafrost temperatures (up to 1.5°C at a 20-m depth over a period of 15 yr) for the area has been reported by Osterkamp and Romanovsky (1996) and Stieglitz et al. (2003a). These trends imply a changing water budget in the KRB.

b. Water budget

The water budget for the KRB may be expressed as

$$P = R + E + \Delta S, \quad (1)$$

where P is precipitation, R denotes river runoff, E represents evapotranspiration, and ΔS is a change in soil moisture (positive for a net gain of soil moisture). The evapotranspiration rate can further be partitioned into three distinct components: evapotranspiration with snow-free conditions ET (including bare soils, lakes, and vegetation), surface sublimation from the snowpack E_s, and aeolian sublimation during blowing snow E_a. All terms are expressed here in units of millimeters per year. McNamara et al. (1998) provide values of P = 262 mm yr^{-1} and R = 139 mm yr^{-1} based on observations collected during 3 yr (1993–95). If no change in soil moisture (i.e., ΔS = 0) is assumed over this time period, this implies that E = 123 mm yr^{-1}. The following paragraphs summarize previous work investigating the KRB's water budget and the physical processes involved.

c. Summary of previous work

Scientific research spurred by interest in high-latitude processes has led to the deployment of an extensive meteorological and hydrological network throughout the basin in recent decades. The availability of observational data has provided a better understanding of the KRB's climate, environment, and water budget. For instance, Zhang et al. (1996) characterized the climate of the basin by investigating the spatial variation of the observed air temperature and precipitation along a north–south transect on the North Slope of Alaska. Olsson et al. (2003) classified the Alaskan Arctic cold season into five stages by analyzing point observations of air and ground temperatures, snow, and soil moisture over two years. König and Sturm (1998) used aerial photography and topographic relationships to map snow on the North Slope of Alaska. Taras et al. (2002) analyzed snow–ground interface temperatures measured along a north–south transect in the KRB. Shiklomanov and Nelson (1999, 2002) determined the spatial variation of the active layer during summer in the Kuparuk region. Other research has addressed soil freeze/thaw processes and their role on hydrological processes in the area (Hinzman et al. 1991; Kane et al. 1991b; Osterkamp and Romanovsky 1997; Romanovsky and Osterkamp 1997). Observational studies of permafrost temperatures on the North Slope of Alaska were conducted by Osterkamp and Payne (1981), Osterkamp and Romanovsky (1996), and Stieglitz et al. (2003a), among others. A comprehensive analysis of the KRB's water budget based on observations of precipitation and river runoff is provided by McNamara et al. (1998). Measurements of evapotranspiration have focused on small-scale North Slope watersheds (Kane et al. 1990, 1991a; Mendez et al. 1998). A complete synthesis of KRB observations is given by Kane et al. (2000).

Numerical studies of the KRB have generally focused on a single process affecting the water budget. This includes the investigation of snow and its redistribution by wind (Liston and Sturm 2002; Bowling et al. 2004; Déry et al. 2004), and of soil and permafrost temperatures (Hinzman et al. 1998; Stieglitz et al. 1999, 2003a). Hydrologic and ecohydrologic simulations have focused on smaller, nested watersheds of the KRB including the 2.2-km^2 Imnavait Creek (Hinzman and Kane 1991, 1992; Ostendorf et al. 1996; Quinn et al. 1998; Stieglitz et al. 1999, 2003b) and the 142-km^2 Upper Kuparuk River basin (Zhang et al. 2000; Déry et al. 2004). We expand on this previous work by examining atmospheric and land surface processes over the entire KRB for an extended period of 11 yr (1991–2001) to better capture some of the temporal and spatial variability in the components of the water budget. In the application of a land surface model, we fully simulate the dynamical evolution of the three terms on the right-hand side of Eq. (1). Results from our analyses and numerical simulations are presented after a description of the model and the datasets used in this study.

3. Catchment-based Land Surface Model

a. Original model framework

Owing to the lack of an extensive observational network of soil moisture and evapotranspiration in the KRB, the National Aeronautics and Space Administration's (NASA) Seasonal-to-Interannual Prediction Project (NSIPP) Catchment-based Land Surface Model (CLSM) is used to simulate land surface processes and their interactions with the atmosphere (Koster et al. 2000; Ducharne et al. 2000). Although developed for application within the NSIPP general circulation model (GCM), the CLSM is operated "offline" in this study since a comprehensive meteorological dataset is available for the KRB (see section 4). The standard meteorological variables of the near-surface air temperature T (K), the relative humidity RH (%), the wind speed U (m s^{-1}), the surface atmospheric pressure P_s (hPa), and the incoming solar $K^{\downarrow}$ and longwave $L^{\downarrow}$ radiation (W m^{-2}) constitute the main driving variables. Furthermore, the precipitation rate P (mm h^{-1}) is the only term in the water budget that is prescribed in this case; all others compose prognostic quantities in the stand-alone version of the CLSM. The methodology by which the remaining terms in the water budget are evaluated in the CLSM follows.

In contrast to traditional land surface schemes, the CLSM employs the watershed as the fundamental hydrologic unit instead of a rectangular grid cell. In each catchment unit, TOPMODEL (Beven and Kirkby 1979) equations are applied to relate the soil moisture distribution to topography. The application of a TOPMODEL-based land surface model requires several assumptions including that 1) the saturated hydraulic conductivity decays exponentially with depth; 2) a steady state between recharge and subsurface flow exists; and 3) the water table is parallel to the soil surface (Beven 1997). The environmental conditions of the KRB justify these assumptions. Soils are relatively thin and there is a sharp topographic gradient from the headwaters of the KRB to the Arctic Ocean. In addition, the saturated hydraulic conductivity of the top organic soil layer has been measured to be 10 to 1000

FIG. 1. (a) Geographical map of Alaska, the Kuparuk River basin (shaded), and surrounding features. (b) Close-up map of the Kuparuk River basin, including the 13 subbasins over which the CLSM is run and contours of elevation.

times greater than that of the mineral soil layers below it (Hinzman et al. 1991, 1996).

Statistics of the topographic index (TPI), defined as ln (a/tanβ), where a is the upstream contributing area to a downslope point with a local slope tanβ, provide the means by which three different soil moisture regimes are identified in a catchment. The different zones are specified as a saturated area (high TPI values), an unsaturated area (intermediate TPI values), and a wilting area (low TPI values). Rainfall or snowmelt onto the saturated fraction contributes directly to surface runoff. Baseflow associated with lateral flow in the water table contributes additional runoff during summer. For the evaluation of this component, a singular value of f, the exponential decay of the saturated hydraulic conductivity with depth, is used for each subbasin in the simulations. The total runoff simulated by the CLSM is insensitive to variations in f since surface runoff domi-

(b)

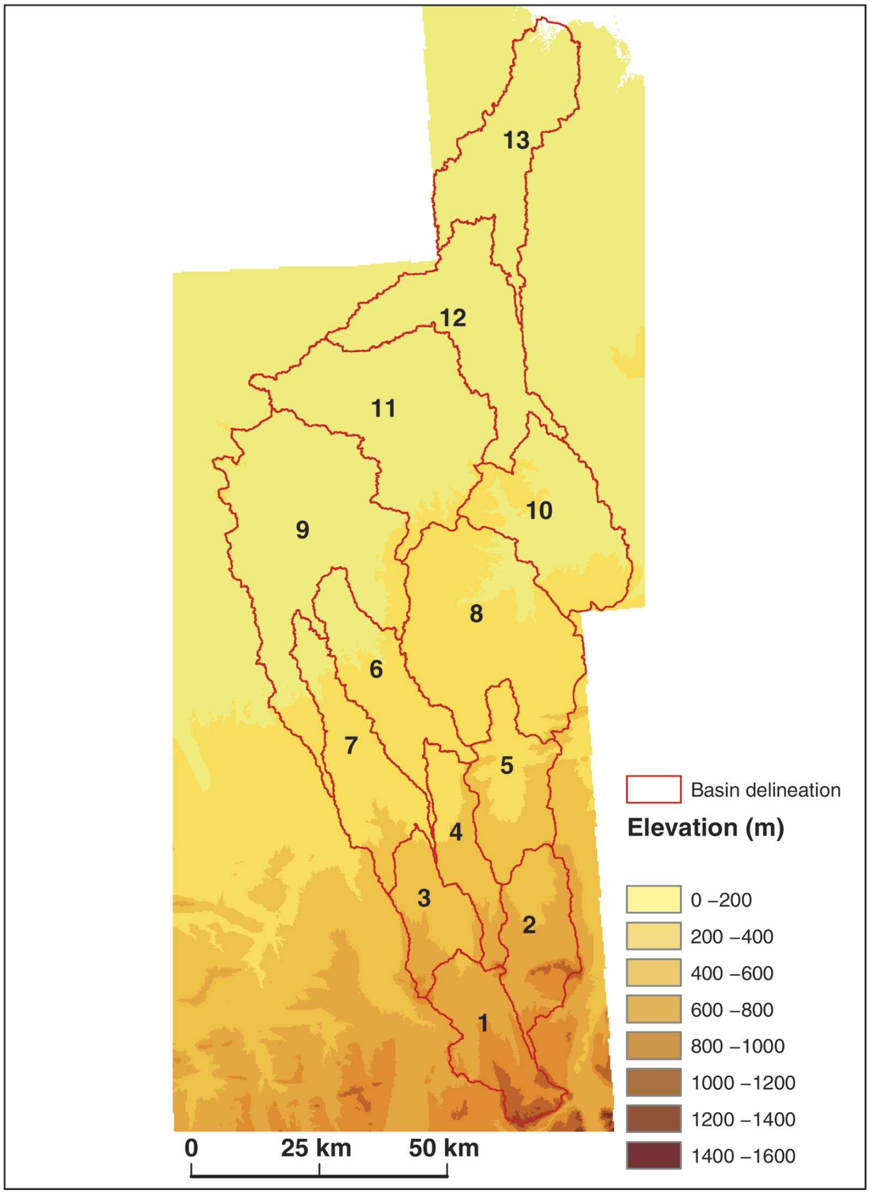

Fig. 1. (*Continued*)

nates the hydrologic regime of this watershed. The shallow active layer and the high evapotranspiration rates during summer are factors that limit the contribution of baseflow to total runoff.

The CLSM evapotranspiration scheme follows from the Mosaic land surface model (Koster and Suarez 1996). The scheme includes transpiration from the vegetation canopy and soil-based evaporation. Evapotranspiration rates are computed separately for the three soil moisture regimes considered by the CLSM (Koster et al. 2000). In the saturated zone, evapotranspiration rates meet the atmospheric demand, as soil moisture is readily available. In the unsaturated fraction of the catchment, potential evapotranspiration rates are reduced by a factor that depends on the soil moisture content. Finally, in the wilting zone, plant transpiration shuts off such that this component no longer contributes to the evaporative fluxes. During winter, surface sublimation from the snowpack supplies additional moisture to the atmosphere and to the total annual evapotranspiration rates. In all instances, potential evapotranspiration or sublimation is computed us-

TABLE 1. The geographical coordinates, area, mean elevation, mean distance, and delay to the outlet, and mean TPI for each of the 13 subbasins in the KRB. The number of each basin refers to its location in Fig. 1b.

Subbasin	Lat (°N)	Lon (°W)	Area (km^2)	Elev (m)	Distance (km)	Delay (days)	TPI
1	68.64	149.48	424	824	199	5	7.71
2	68.80	149.23	411	696	179	4	7.94
3	68.86	149.73	318	566	176	4	8.04
4	68.97	149.56	311	474	162	4	8.24
5	69.09	149.29	428	413	148	3	8.15
6	69.27	149.91	497	237	137	3	8.65
7	69.14	150.05	523	296	149	3	8.55
8	69.36	149.40	1084	261	119	3	8.35
9	69.52	150.24	1307	150	113	3	8.84
10	69.53	149.02	690	185	98	2	8.53
11	69.72	149.76	1031	118	84	2	8.87
12	69.88	149.39	737	77	63	1	9.62
13	70.18	149.01	660	24	26	1	10.54
Total	. . .	. . .	8421	. . .	. . .	. . .	. . .
Mean	69.30	149.54	648	263	127	3	8.62

ing standard bulk formulas that rely on vertical gradients of water vapor and wind speed (e.g., Oke 1987). The areal average of the evaporative fluxes from each soil moisture regime provides the total latent heat flux for a given watershed.

The CLSM prognostic variable that represents the spatially integrated soil moisture content is the catchment deficit M_D (mm) (Koster et al. 2000). This variable denotes the amount of water that a given watershed can absorb before it becomes entirely saturated; large (small) values of M_D correspond to relatively dry (wet) soil conditions. Thus a change in catchment deficit equates, in absolute terms, to a change in soil moisture, that is, $|\Delta M_D| = |\Delta S|$. This includes storage in lakes and wetlands that is represented by a change in the saturated fraction of a basin (Koster et al. 2000). The amount of water stored as soil moisture in the catchment increases with the infiltration of rainfall or snowmelt, but decreases with river runoff and evapotranspiration.

b. *Recent modifications and application to the North Slope of Alaska*

Since winter dominates the climate of the KRB, snow and ice play a critical role in its water budget. Therefore, the CLSM is coupled to both a snow physics model and a ground/permafrost thermodynamics scheme. The snow physics model simulates the evolution of the heat content, snow water equivalent, and snow depth for each of *n* layers in the snowpack (Lynch-Stieglitz 1994; Stieglitz et al. 2001). Processes considered by the snow model include precipitation, sublimation, snowmelt, compaction, liquid water infiltration, and refreezing. However, it does not account for the horizontal transport of snow by wind that leads to significant small-scale heterogeneity in the end-of-winter snow cover. This nonuniformity in the snow cover has significant impacts on the energy and water budgets during the spring transition period (e.g., Luce et al. 1998; Déry et al. 2004). To avoid the use of distributed and numerically expensive blowing-snow models (e.g., Liston and Sturm 1998; Déry et al. 1998; Xiao et al. 2000), a parameterization that divides the watershed into two zones, one with a shallow snowpack representing zones where winds erode snow from the surface, and another with a deep snowpack where winds deposit the blowing snow, is implemented in the CLSM (Déry et al. 2004). Typically, erosion areas are found on windward slopes and on ridges, whereas deposition areas are found on lee slopes and in valleys (Liston and Sturm 1998). Snow areal depletion curves inferred from the Moderate Resolution Imaging Spectroradiometer (MODIS) are used to determine the shallow and deep snow-cover fractions (Déry et al. 2005). Blowing-snow sublimation enhances the surface latent heat flux during high-wind events (Déry and Yau 2001a) and is evaluated with a parameterization developed by Déry and Yau (2001b). Aeolian sublimation occurs when environmental conditions are conducive to blowing snow (Déry and Yau 1999, 2002) and is assumed to occur only over the shallow snowpack area where winds erode snow from the surface. The abundance of snow in riverine depressions owing to wind redistribution retards the onset of significant river runoff during the early stages of snowmelt (Kane et al. 2000; Zhang et al. 2000). To account for the effects of snow damming, the CLSM subgrid-scale snow scheme now transfers all meltwater from the shallow snowpack to the deep snowpack instead of delivering the water directly to surface runoff and/or to ground infiltration. Unless the added water surpasses the liquid water holding capacity of ≈5% by height of a layer thickness (Jordan 1991; Lynch-Stieglitz 1994), then it remains in the snowpack and hence runoff is delayed.

The subsurface thermodynamics model resolves freeze/thaw processes and heat transfer between soil layers using a linear heat diffusion scheme (Stieglitz et al. 2001). This provides for a proper evolution of the seasonal thaw depth of the active layer, which is defined as the thickness of the soil layer that is situated just below the ground/atmosphere interface but above the permafrost table and that is characterized by above-freezing temperatures for a period of time each year (French 1993). Frozen subsurface layers in the permafrost table hinder deep water infiltration and do not contribute to the simulated baseflow. During summertime, the thaw front deepens such that a larger fraction of the soil column becomes hydrologically active. At this stage, shallow subsurface layers (above the water table) may approach saturation during rainstorms. Instead of infiltrating deeper into the ground, the water in these shallow layers is allowed to move laterally, thereby contributing directly to runoff (Shaman et al. 2002). The CLSM assumes spatially uniform depth-to-mineral soil in its calculation of the maximum catchment deficit. In the headwaters of the KRB, however, the depth-to-mineral soil varies from 0.1 m at ridge tops to 0.75 m in valley bottoms (Hinzman et al. 1991, 1996; Kane et al. 1991a; McNamara et al. 1997; Walker and Walker 1996). The baseflow parameters in the CLSM are modified to account for this spatial variability (Ducharne et al. 2000). The CLSM then becomes more responsive to summertime rainstorms by reducing the overall capacity of soils to retain water (Shaman et al. 2002; Stieglitz et al. 2003b). Since the CLSM currently imparts runoff directly from the hillslope to the catchment outlet and does not include interactions between upstream and downstream subbasins, we apply a "delay scheme" to represent the effects of river routing on the total, areally averaged discharge for the Kuparuk River. The scheme assigns a delay (in days) to each of the 13 subbasins according to the distance between its geographical center to the outlet of the Kuparuk River (see Table 1). To this end, an effective flow speed of 0.5 m s^{-1} is used following the optimal values employed in other river modeling studies (e.g., Miller et al. 1994). This effective flow speed yields delays that range from 1 day for subbasin 13 to 5 days for subbasin 1 in the calculation of the total, areally averaged discharge for the KRB.

4. Datasets

a. Digital elevation model

The CLSM requires information on several topographic parameters (see section 3). To this end, a high-resolution digital elevation model (DEM) of the Kuparuk watershed has been acquired (Nolan 2003). Using the DEM, the KRB is divided into 13 subbasins to provide a better representation of the north–south gradient in topography (Fig. 1b). Statistics of the topographic index for each basin were then generated based on a 25-m-resolution DEM and are provided in Table 1. A three-parameter gamma distribution was then fit to the data and the first three moments of this function serve as input into the CLSM (Sivapalan et al. 1987; Ducharne et al. 2000). Other geographical statistics for the 13 subbasins are listed in Table 1.

b. Meteorological observations

The KRB has been the scene of multiple field studies in the past 15 yr that have required comprehensive meteorological and river discharge records. Since 1985, a dozen or so meteorological stations have been mounted in the region as part of the Water and Environmental Research Center North Slope Hydrology Research Project at the University of Alaska Fairbanks (Kane et al. 2002). Three Wyoming snow gauges operated by the Natural Resources Conservation Service supply essential information on wintertime snowfall. The installation of the Arctic Long-Term Ecological Research (LTER) station at Toolik Lake provides further meteorological information from 1988 to the present.

To force the CLSM, data from these 18 meteorological sites located in the vicinity of the KRB are utilized (Table 2). The period chosen for this study begins on 1 January 1991 and ends on 31 December 2001, for a total of 11 yr. Although meteorological records are available prior to 1991, some of the data remain sparse (especially radiation measurements during the winter) and so are not used in this study. All standard meteorological variables required to drive the CLSM (see section 3) are available on an hourly basis. This includes conditions of T, RH, U, P_s, P, and $K^{\downarrow}$; however, significant gaps in $L^{\downarrow}$ are found such that this quantity is estimated as (Jones 1992)

$$L^{\downarrow} = \sigma(T - 20)^4, \tag{2}$$

where σ ($=5.678 \times 10^{-8}$ W m^{-2} K^{-4}) is the Stefan–Boltzman constant. The lack of upper-air humidity or cloud measurements in the observational databases requires the use of this simple formulation for $L^{\downarrow}$.

Daily snowfall rates from the three Wyoming snow

TABLE 2. List of the meteorological stations in the vicinity of the Kuparuk River basin of Alaska, their abbreviations, geographical coordinates, elevation, and associated meteorological fields (even if only partially available throughout the period 1991–2001). The measurements of surface air temperature (T), relative humidity with respect to water (RH), wind speed (U), surface atmospheric pressure (P_s), incoming shortwave ($K^{\downarrow}$) and longwave ($L^{\downarrow}$) radiation, snowfall (S_n), and precipitation rate (P) are listed where available. The data are taken from Kane et al. (2002), Kane and Hinzman (2003), the Arctic LTER database (http://ecosystems.mbl.edu/arc/), and the Natural Resources Conservation Service (http://www.wcc.nrcs.usda.gov/).

Station	Abbreviation	Lat (°N)	Lon (°W)	Elev (m)	Available fields
Atigun Pass	AT	68.13	149.48	1463	S_n
Betty Pingo	BM	70.27	148.88	12	P, RH, T, U
East Headwater	EH	68.57	149.30	909*	P, T, U
Franklin Bluffs	FB	69.83	148.60	78	$K^{\downarrow}$, $L^{\downarrow}$, RH, T, U
Green Cabin Lake	GL	68.53	149.22	975*	P, T, U
Imnavait Creek	IA	68.62	149.28	910	$K^{\downarrow}$, $L^{\downarrow}$, P, P_s, RH, S_n, T, U
Lower Kuparuk	LK	70.28	148.97	78	$K^{\downarrow}$, $L^{\downarrow}$, P, RH, T, U
North Headwater	NH	68.60	149.42	944*	P, T, U
North Prudhoe Bay	NP	70.35	148.52	23**	RH, T
Sagwon	SH	69.42	148.75	299	$K^{\downarrow}$, $L^{\downarrow}$, P, RH, S_n, T, U
Toolik Lake	TK	68.63	149.60	900	$K^{\downarrow}$, P, P_s, RH, T, U
Upper Headwater	UH	68.52	149.33	1003*	P, T, U
Upper Kuparuk	UK	68.63	149.40	774	P, RH, T, U
West Dock	WD	70.37	148.55	8	$K^{\downarrow}$, $L^{\downarrow}$, P, RH, T, U
West Headwater	WH	68.55	149.40	1018*	P, T, U
West Kuparuk	WK	69.42	150.33	160	$K^{\downarrow}$, $L^{\downarrow}$, P, P_s, RH, T, U

* Data taken from the "Elevation Finder" available online at http://216.27.181.157/elevation/Elevation.asp.
** Data taken from Zhang et al. (1996).

gauges are divided by 24 to provide hourly wintertime precipitation rates, but are multiplied by a factor of 1.25 to account for wind undercatch and wetting losses (Yang et al. 2000). The loss of the Wyoming snow gauge at Sagwon in 1997 affected significantly the observed snowfall rates in the northern subbasins of the KRB. Missing snowfall rates for Sagwon are therefore estimated from the 1991–96 climatological values for Sagwon only. The approximate accuracy in the measurement of each variable is given in Table 3.

The forcing data are then interpolated onto each of the 13 subbasins in the KRB by linearly weighting each of the available stations inversely to the square of its distance from the center of the subbasin. If data are

TABLE 3. Measured values of the mean annual surface air temperature (T), relative humidity with respect to water (RH), relative humidity with respect to ice (RH$_i$), 10-m wind speed (U_{10}), surface atmospheric pressure (P_s), and incoming shortwave ($K^{\downarrow}$) and longwave ($L^{\downarrow}$) radiation, as well as the total yearly precipitation (P), snowfall (S_n), and river runoff (R) for the Kuparuk River basin from 1991 to 2001. Note that values of RH$_i$ are computed only when $T < 0°$C. The approximate accuracy of the meteorological measurements based on the instrumentation mounted at the Arctic LTER is given for each variable (http://ecosystems.mbl.edu/arc/).

Year	T (°C)	RH (%)	RH$_i$ (%)	U_{10} (m s^{-1})	P_s (hPa)	$K^{\downarrow}$ (W m^{-2})	$L^{\downarrow}$ (W m^{-2})	P (mm)	S_n (mm)	R (mm)
Accuracy	±1°C	±3%	±3%	±1.5%	±0.3 hPa	±3%	±1%	±1%	±1%	±15%*
1991	−9.6	74.8	88.1	3.3	926.0	105.8	205.2	328.0	200.1	111.8
1992	−10.4	76.0	94.4	3.6	888.5	103.4	203.5	301.7	154.5	135.7
1993	−7.2	79.9	95.5	4.0	888.7	94.8	217.9	281.0	127.2	159.8
1994	−10.1	76.6	91.1	3.7	910.5	98.6	205.5	340.1	172.7	140.6
1995	−8.9	80.6	94.3	3.7	912.5	93.5	206.3	270.7	110.3	168.2
1996	−10.1	80.8	95.9	3.9	908.4	93.5	203.5	299.2	139.2	180.7
1997	−10.0	81.6	97.9	3.7	909.4	98.4	204.2	318.2	119.7	247.5
1998	−7.7	80.4	95.0	3.5	921.3	95.7	211.1	245.6	85.6	128.5
1999	−11.4	77.3	91.9	3.4	919.9	101.8	199.3	336.0	108.1	139.2
2000	−10.1	82.2	97.0	3.5	920.7	106.5	203.2	232.2	101.1	181.9
2001	−9.9	80.6	95.3	3.3	919.2	107.3	203.6	264.9	111.1	151.3
Mean	−9.6	79.2	94.5	3.6	911.4	99.9	205.7	292.5	130.0	158.7

* The USGS monthly streamflow data for the Kuparuk River are qualified as "fair." This implies that 95% of the measured monthly discharge rates are within ±15% of the actual values (D. F. Meyer 2004, personal communication).

nonexistent or missing for a particular location and time, then that station does not contribute to the weighting scheme and more emphasis is given to other locations. This approach yields continuous time series for all of the required forcing variables while providing variations in these quantities that are more typical of the local topography and climate. However, the air temperatures are not adjusted to account for vertical lapse rates.

c. Discharge

Another dataset used in this study consists of discharge data recorded by the United States Geological Survey (USGS) at Deadhorse, Alaska. This site is located near Prudhoe Bay and provides a comprehensive dataset of river discharge at the mouth of the Kuparuk for the period 1971 to the present. The discharge rates are expressed in units of millimeters per day for comparison with other terms in the water budget. In addition, the discharge rates form an independent dataset by which the hydrologic simulations can be validated.

5. Analyses of observations

Table 3 provides the mean annual conditions over the KRB for each of the variables used to drive the CLSM. Additional information on the relative humidity with respect to ice (evaluated only when air temperatures are subfreezing) and on river runoff (as measured at Deadhorse, Alaska) is included in Table 3. Our analysis focuses on the air temperature and the water budget terms.

The mean annual air temperature in the KRB over the period 1991–2001 is −10°C, matching the climatological norms reported by Zhang et al. (1996) for the region. The interannual variability in the mean annual air temperature is about ±2°C. Figure 2 illustrates the pronounced latitudinal gradient in mean annual air temperature that exists in the KRB. Even with their higher elevations, the southernmost subbasins of the KRB are warmer on average by 2.5°C compared to their northern counterparts.

The mean annual precipitation amounts to 292 mm (Table 3). The consideration of an undercatch factor in this study enhances the annual precipitation totals from the 262 mm yr^{-1} reported by McNamara et al. (1998). As a result of orographic lifting, mean annual precipitation totals in the southern parts of the KRB are nearly double those found near the Arctic coastline (Fig. 3a). This sharp north–south gradient in precipitation is well documented (Zhang et al. 1996; Kane et al. 2000). Snowfall accounts for 44% of the mean annual precipitation totals measured in the KRB (Table 3). Solid precipitation also reaches a maximum in the southern locales of the KRB, despite the colder air temperatures observed near the Arctic coastline (Fig. 3b). For the entire KRB, snowfall amounts equate to 130-mm swe per year.

In the investigation of the water budget for the KRB, it is of importance to identify the mean conditions as well as extremes of the climatic state. To this end, the normalized precipitation anomaly (NPA) and the normalized temperature anomaly (NTA) are computed. These are defined as

$$\mathrm{NPA} = \frac{P_i - \overline{P}}{s_P} \tag{3}$$

and

$$\mathrm{NTA} = \frac{T_i - \overline{T}}{s_T}, \tag{4}$$

where the subscript i denotes an individual year, the overbar denotes the annual average value for the period 1991–2001, and s denotes the standard deviation for precipitation or temperature. Following Barber et al. (2000), we then calculated the difference between NPA and NTA. A positive (negative) value of this difference, hereafter referred to as a "climate index," infers a cool and wet (warm and dry) year. Figure 4a depicts the correspondence between the total annual precipitation and mean annual air temperature. Over the 11-yr period, there is a negative correlation ($R = -0.49$, with probability = 0.13) between these two quantities. In other words, warm years tend to be dry (negative climate index values) and cool years tend to be wet (positive climate index values). Figure 4b illustrates that 1993 and 1998 stand out as relatively warm, dry years, whereas 1999 represents a relatively cool, wet year. The climate index provides a simple measure of the interannual variability in observed meteorological conditions and in the simulated water budget terms. The applicability and utility of the climate index are demonstrated in section 7.

River runoff provides an integrated measure of the KRB's response to the atmospheric supply of precipitation and demand of surface moisture through evapotranspiration. On average, 54% of the annual precipitation runs off in the KRB, suggesting that evapotranspiration reaches 134 mm yr^{-1} if the change in soil moisture is considered to be zero over the period of record (Table 3). As with precipitation, river runoff exhibits significant interannual variability. If all snowfall is entirely converted into runoff, it provides 82% of

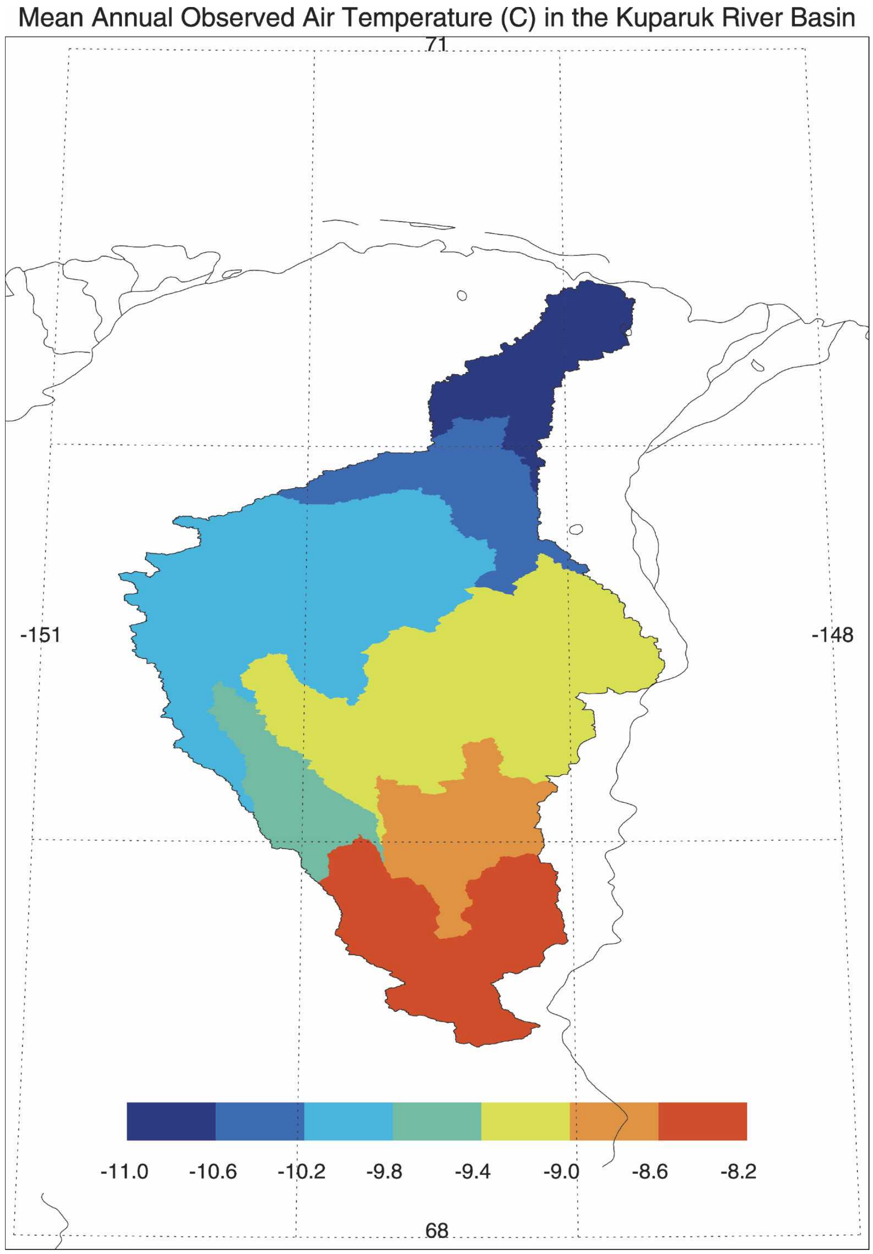

FIG. 2. The observed mean annual air temperature (°C) in the Kuparuk River basin, 1991–2001.

the annual river runoff, in agreement with the findings of McNamara et al. (1998).

6. Numerical results

Numerical simulations conducted with the CLSM provide the necessary information to derive the spatial and temporal variability of those processes affecting the water budget of the KRB. The model is spun up over a period of 30 yr using 1991 observational data until steady states for the water and energy balances have been achieved for each of the 13 subbasins. The hourly meteorological data are linearly interpolated to each 20-min time step and used to run the model forward. For the integrations, the CLSM snow module employs three dynamic snow layers and considers subgrid-scale snow heterogeneity. The mean areal fractions covered by the shallow (76%) and deep (24%) snow covers are supplied by MODIS analysis (see Déry et al. 2005). For each prognostic quantity, the results are averaged ac-

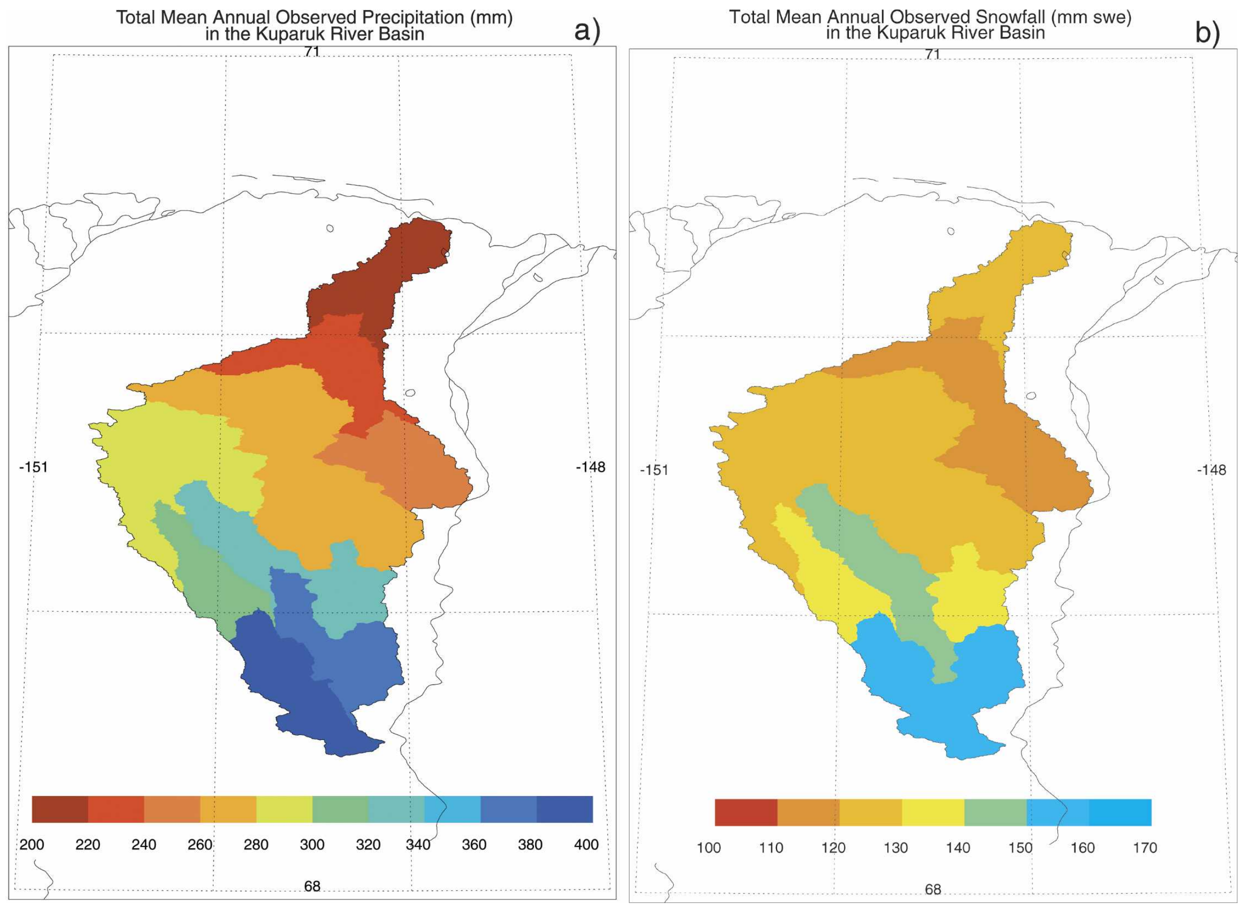

FIG. 3. The observed mean annual (a) precipitation (mm) and (b) snowfall (mm swe) in the Kuparuk River basin, 1991–2001.

cording to subbasin size to provide the total or mean values for the entire KRB.

a. Model validation

Figure 5 presents a comparison of the observed and the simulated daily discharge rates for the Kuparuk River between 1 May and 30 September of each year of interest. Runoff during the winter months is not shown as it is near zero at all times. From this comparison, it is evident that runoff associated with snowmelt is the most significant hydrologic event of the year and occurs in May and June. The CLSM captures the timing and intensity of this event well and accurately depicts summer and early fall runoff associated with rainstorms.

Table 4 provides the coefficient of determination, mean absolute error, and root-mean-square error based on the 1 May to 30 September observed and simulated river runoff rates. Averaged over the 11 yr, the mean absolute and root-mean-square errors attain values of 0.83 and 0.14 mm day^{-1}, respectively. The mean coefficient of determination equals 0.41, although it ranges from 0.87 in 1992 to 0.05 in 2001. The model's ability to depict interannual variability in the observed runoff is discussed further in section 7. The final panel in Fig. 5 shows that the mean climatology of daily runoff is also well simulated by the CLSM. The mean annual total observed and simulated river runoff rates are 159 and 169 mm, respectively. This suggests that the model generates 6% more river runoff than is observed in the KRB.

b. River runoff, evapotranspiration, and sublimation

The simulated river runoff rates for each of the 13 subbasins are provided in Fig. 6. The maximum river discharge rates per contributing area amount to 240 mm yr^{-1} and are observed in the southernmost subbasins of the KRB where precipitation attains a basinwide annual maximum. This is also the region of relatively low TPI values and steep slopes, factors that enhance the response of the watershed to precipitation input. Moving northward, there is a progressively diminishing

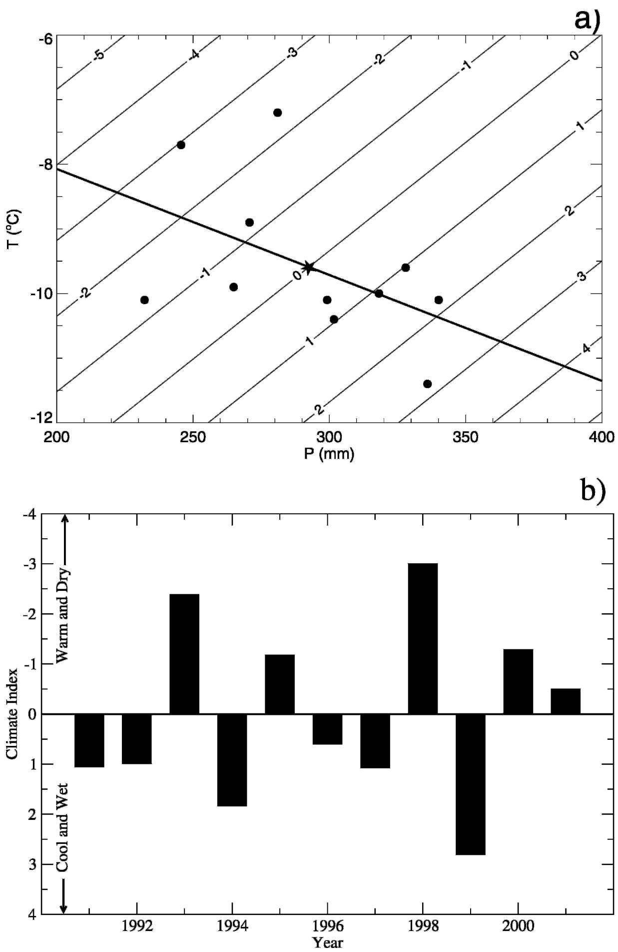

FIG. 4. (a) The total annual precipitation (P) vs the mean annual surface air temperature (T) for the Kuparuk River basin, 1991–2001 (black circles). The star depicts the 11-yr mean, and the contours denote lines of equal climate index values (see text for details). Statistics for the linear regression (thick black line) are given in Table 7. (b) The temporal evolution of the climate index for the Kuparuk River basin, 1991–2001.

contribution per area of the subbasins to total river discharge. A minimum discharge of 122 mm yr^{-1} is found in subbasins 12 and 13 where flat terrain and low precipitation rates constrain runoff.

Total evapotranspiration rates simulated by the CLSM are presented in Fig. 7a. Similar to the runoff rates, evaporative fluxes are greatest at the southern end of the KRB where the mean annual total evapotranspiration approaches 150 mm. This is in good agreement with the 163 mm yr^{-1} in evapotranspiration measured by Kane et al. (1990) for Imnavait Creek during 1986–89. The maximum in the evaporative fluxes coincides with the areas where the largest mean annual precipitation totals are observed (cf. Fig. 3a). Most of the evapotranspiration occurs during the warm season (June to August; Fig. 7b), with surface-snow and blowing-snow sublimation accounting for no more than a few millimeters of the total evaporation rates each year across the KRB (Figs. 7c and 7d). Blowing-snow sublimation accounts for about half of the wintertime sublimation rates across the KRB. Although snow covers the surface for more than two-thirds of the year, the combined processes of surface-snow and blowing-snow sublimation account for no more than 5% of the total yearly evaporative fluxes and a sink of 2% of the total annual precipitation in the KRB.

c. *Soil moisture*

Figure 8 illustrates the interannual variability in soil moisture over the 11-yr period. Relatively warm, dry years (such as 1998; cf. Fig. 4) induce a negative change in ΔS, indicative of drying in the KRB. On the other hand, a positive value of ΔS, as experienced in 1999, implies a recharge in soil moisture associated with a relatively cool, wet year. The anomalous result obtained for 1993 arises from the seasonal nature of the temperature and precipitation departures that year (see further discussion in section 7). The range in ΔS of ± 18 mm yr^{-1} signifies that a change in soil moisture can account for $\pm 7\%$ of the water budget is any given year, although the long-term contribution of this term approaches zero.

The intensity of the precipitation, evapotranspiration, and river runoff rates determine the soil moisture conditions of the KRB. Figure 9 depicts the spatial distribution of the mean annual catchment deficits across the KRB for the period 1991–2001. Large values of M_D denote subbasins where river runoff and evapotranspiration rates are relatively high compared to the precipitation input. The mean annual catchment deficit decreases from the headwater basins moving northward into the foothills of the Brooks Range. From the midsections of the KRB, values of M_D begin to increase moving northward onto the Arctic coastal plain. This pattern is inconsistent with remote sensing data of soil moisture that show a significant fraction of the surface reaches saturation during snowmelt on the North Slope of Alaska (Bowling et al. 2003) and is still under investigation.

d. *Annual cycle*

Figure 10 represents the mean annual cycle of daily air temperature, precipitation, river runoff, evapotranspiration, catchment deficit, thaw depth, and water table depth for the KRB over the period 1991–2001. The annual cycles of daily air temperature and precipitation are derived from observations and river runoff is taken

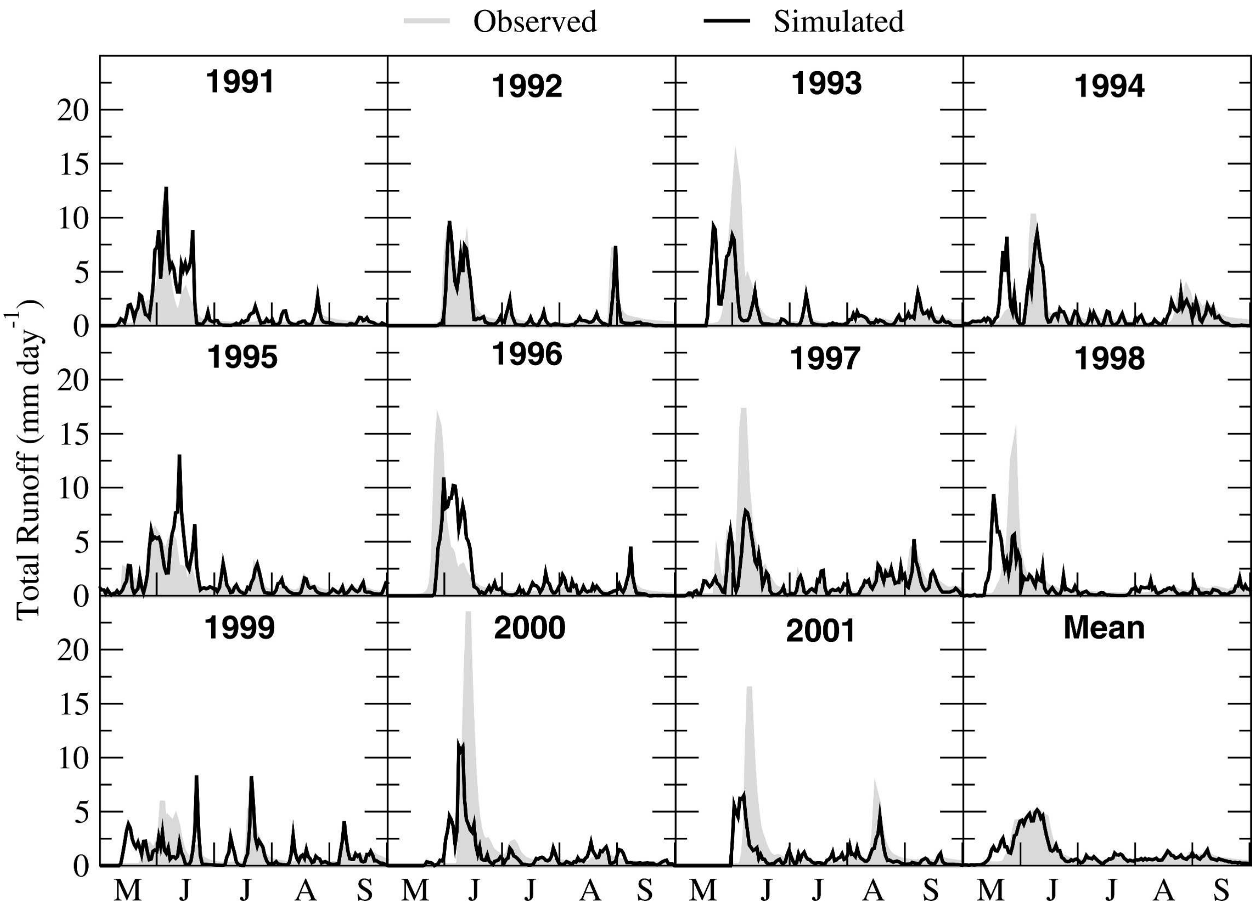

FIG. 5. The observed and simulated daily runoff rates (mm day^{-1}) for the Kuparuk River basin from 1 May to 30 Sep for the period 1991–2001. Mean daily values of runoff over the period 1991–2001 are also included.

from both observations and the numerical experiments, whereas all other quantities are inferred from the CLSM simulations.

Daily air temperatures remain below 0°C for 246 days and reach a minimum of −30°C on average each 16 December (Fig. 10a). Daily air temperatures are at their warmest in July, peaking at 14°C on 16 July. The brief warm season during which above-freezing air temperatures are observed lasts 118 days on average. The southernmost subbasins experience $T > 0$°C a week longer than their northern counterparts.

The mean annual cycle of daily precipitation shows considerable day-to-day variation (Fig. 10b). On average, daily precipitation rates attain a yearly maximum during summer. Snowfall events tend to be lighter owing to the reduced amount of moisture the atmosphere can hold at cold temperatures. The mean annual cycles of the observed and simulated daily runoff rates for the Kuparuk are illustrated in Fig. 10c. Peak discharge rates (≈5 mm day^{-1}) are associated with snowmelt during

TABLE 4. Error analysis for the CLSM simulation of river runoff compared to observations recorded by the USGS at Deadhorse, AK. The analysis is based on the daily values of river runoff over the period 1 May to 30 Sep of each year for 1991–2001. The following abbreviations are used: R^2, coefficient of determination; MAE, mean absolute error; rmse, root-mean-square error.

Year	R^2	MAE (mm day^{-1})	Rmse (mm day^{-1})
1991	0.75	0.75	0.11
1992	0.87	0.39	0.05
1993	0.13	1.01	0.19
1994	0.47	0.74	0.10
1995	0.56	0.69	0.11
1996	0.46	0.91	0.17
1997	0.73	0.82	0.12
1998	0.20	0.75	0.15
1999	0.15	0.85	0.11
2000	0.11	1.22	0.25
2001	0.05	0.96	0.19
Mean	0.41	0.83	0.14

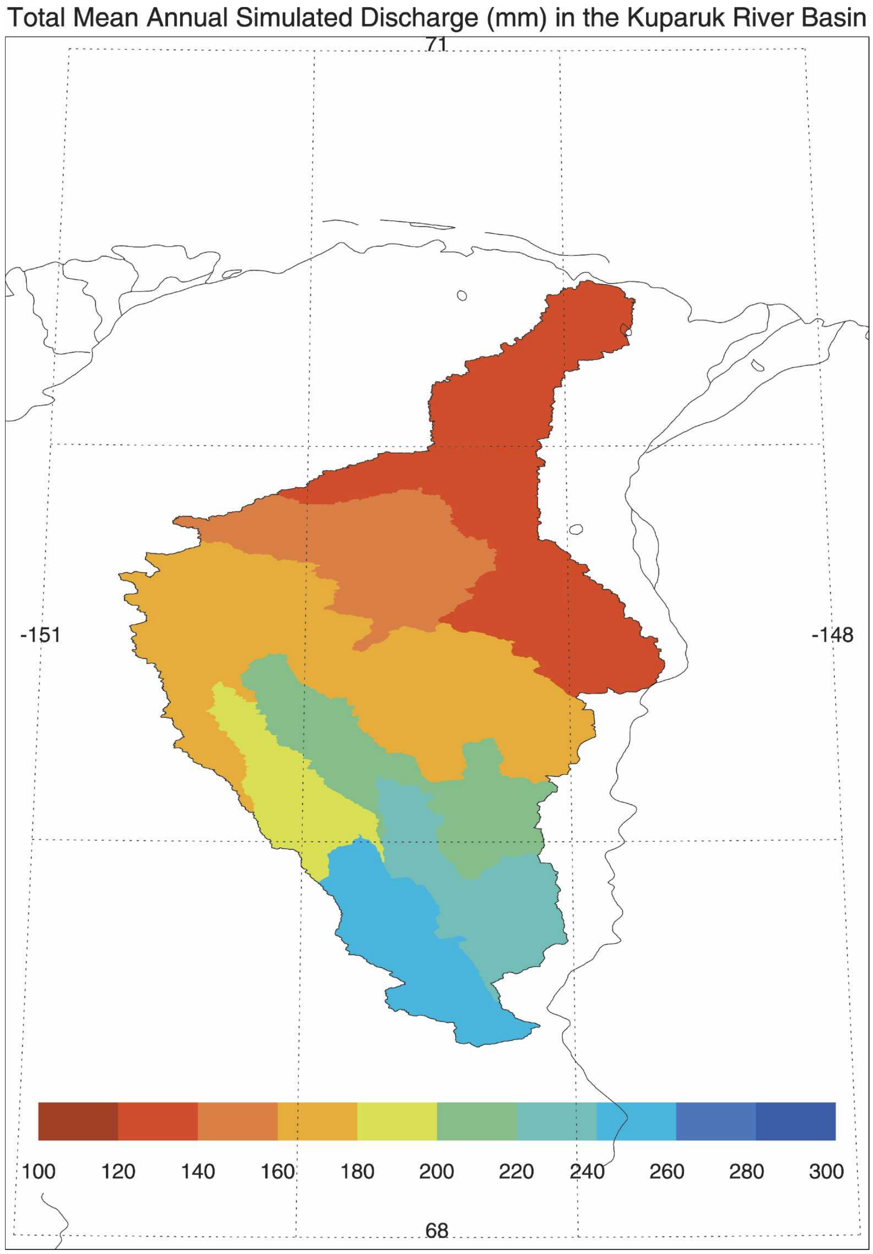

FIG. 6. The simulated mean annual discharge (mm) in the Kuparuk River basin, 1991–2001.

spring, with secondary contributions owing to summertime rainstorms.

The mean annual cycle of evapotranspiration shows minimal values of sublimation/deposition throughout the cold season (Fig. 10d). Significant evapotranspiration ($E > 1$ mm day^{-1}) occurs only after snowmelt. Evaporative fluxes reach a maximum value of 2.6 mm day^{-1} on average each 1 July. From then on, soils begin to dry out such that E slowly diminishes even as air temperatures remain warm and as the atmospheric de-

→

FIG. 7. The simulated mean annual (a) evapotranspiration (mm), (b) snow-free evapotranspiration (mm), (c) surface-snow sublimation (mm), and (d) aeolian sublimation during blowing snow (mm) in the Kuparuk River basin, 1991–2001.

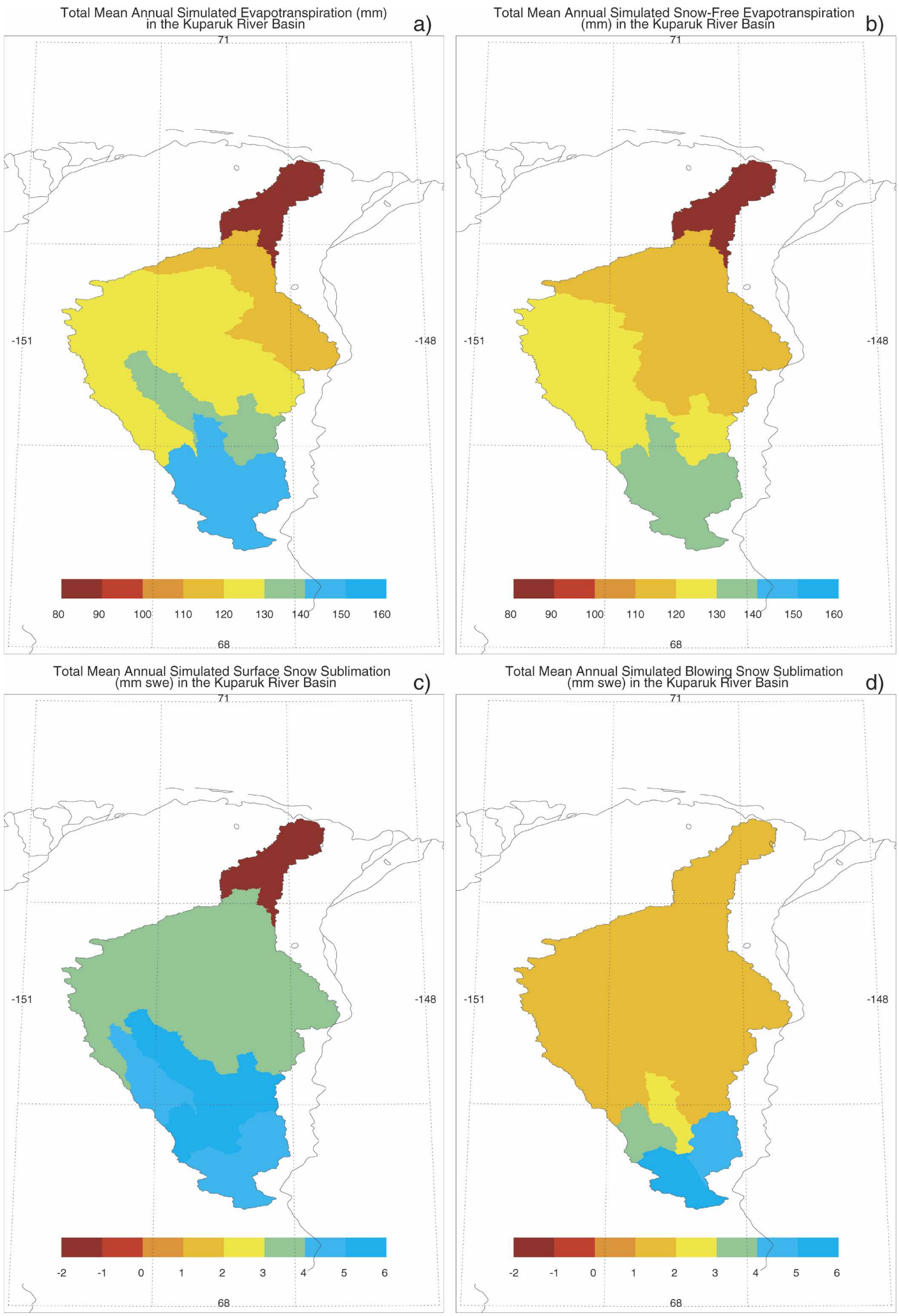
Total Mean Annual Simulated Evapotranspiration (mm) in the Kuparuk River Basin
a)
71
-151
-148
80 90 100 110 120 130 140 150 160
68
Total Mean Annual Simulated Snow-Free Evapotranspiration (mm) in the Kuparuk River Basin
b)
71
-151
-148
80 90 100 110 120 130 140 150 160
68
Total Mean Annual Simulated Surface Snow Sublimation (mm swe) in the Kuparuk River Basin
c)
71
-151
-148
-2 -1 0 1 2 3 4 5 6
68
Total Mean Annual Simulated Blowing Snow Sublimation (mm swe) in the Kuparuk River Basin
d)
71
-151
-148
-2 -1 0 1 2 3 4 5 6
68

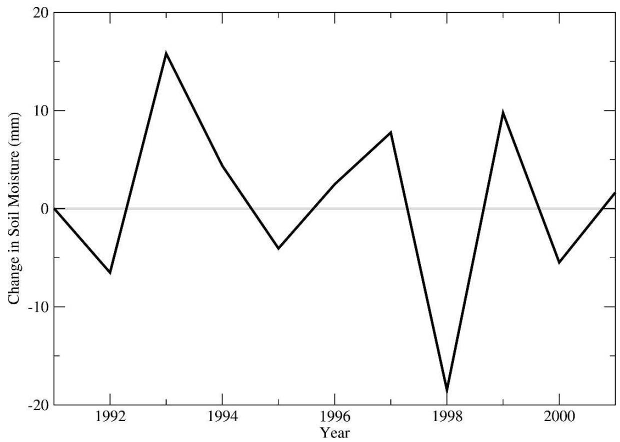

FIG. 8. The annual change in the simulated soil moisture (mm) in the Kuparuk River basin, 1991–2001.

mand is at its greatest. Mean evapotranspiration rates from 1 June to 31 August of each year equate to 1.16 mm day^{-1}. This is only 0.3 mm day^{-1} less than the measured values over the Arctic coastal plain during the summers of 1994–96 (Mendez et al. 1998). The onset of the snow cover in mid-September effectively shuts off most of the evaporation.

Figure 10e illustrates the mean annual cycle of the catchment deficit for the KRB over the period 1991–2001. The annual cycle exhibits little change during winter when discharge is minimal and water is retained in the snowpack as well as in the frozen ground. In late May, there is a rapid decrease in M_D as snowmelt is initiated and replenishes the soil moisture content of the KRB. The soil moisture recharge attains an average of 20 mm yr^{-1} during snowmelt, in accord with the 16 mm yr^{-1} observed in the headwaters of the KRB by Kane et al. (1991a). The minimum value of M_D of 11 mm is attained on average each 10 June. As the summer progresses, evapotranspiration leads to a rapid depletion in the overall soil moisture content, with M_D reaching a maximum value of 45 mm each 30 July. Late summer and early fall rainstorms provide another recharge of soil moisture in the KRB that ends with the onset of subfreezing air temperatures and the snow cover.

Onset of the snowpack occurs in September and gradually increases in swe until late April (Fig. 10f). A maximum of 110-mm swe is retained in the simulated snowpack on average each 7 May. From then on, increasing solar and longwave radiation initiate the melt process that usually occurs over a short period of time. The snow cover completely vanishes on average in mid-June throughout the KRB. MODIS images confirm the tendency for rapid melt periods in the KRB (Déry et al. 2005). The mean annual number of snow-free days, taken as a day that has <5 mm swe or a snow depth of about <2 cm, amounts to 105 days in the KRB. This is within the range of the 102 to 117 snow-free days observed each year on the North Slope of Alaska (Zhang et al. 1996).

The mean annual cycle of daily thaw depth determines the intensity of hydrologic activity in the soil column (Fig. 10g). During winter, the entire soil column stays frozen such that the thaw depth is zero. Following snowmelt in late spring and early summer, there is a rapid warming of the shallow soils that quickly deepens the thaw front. The mean annual maximum thaw depth of 0.81 m is within the range of 0.25 to 1 m reported by Hinzman et al. (1991, 1996). The mean annual maximum thaw depth is reached on average each 2 August, coinciding with the period of the largest catchment deficit. The duration of the period where the thaw depth surpasses 0.1 m is 93 days, an indication of the short growing season that exists in the KRB. Cooler air temperatures beginning in mid-August and continuing into September yield a rapid reduction in the thaw depth. Thereafter, soils remain at 0°C for several weeks since complete freeze-up of the soil column (>99% frozen) does not occur until on average 14 November each year. This slow freezing of the active layer and the timing of freeze-up are consistent with observations (Hinzman et al. 1991; Osterkamp and Romanovsky 1997).

The simulated evolution of the mean daily water table depth (WTD) is inversely proportional to M_D (Fig. 10g). This shows that the mean annual WTD for the entire KRB is 0.83 m. It rises to 0.33 m as snowmelt infiltrates into the ground but is depressed during the summer as evapotranspiration amplifies, reaching a maximum depth of 1.11 m on average each 30 July. Summer and fall rainstorms replenish soil moisture and the WTD rises to its mean value of 0.83 m where it remains constant throughout the winter season.

7. Discussion: Seasonal-to-interannual variability in the KRB water budget and its potential future state

a. Interannual variability

A summary of the observational and numerical results for the water budget of the KRB is presented in Table 5. For the period 1991–2001, precipitation accounts for a mean input of 292 mm yr^{-1} onto the basin. The CLSM simulations partition 58% (169 mm yr^{-1}) of this water into runoff and another 43% (127 mm yr^{-1}) into evapotranspiration. An increase in soil moisture accounts for <1% (1 mm yr^{-1}) imbalance in the simulated water budget. These results correspond well with

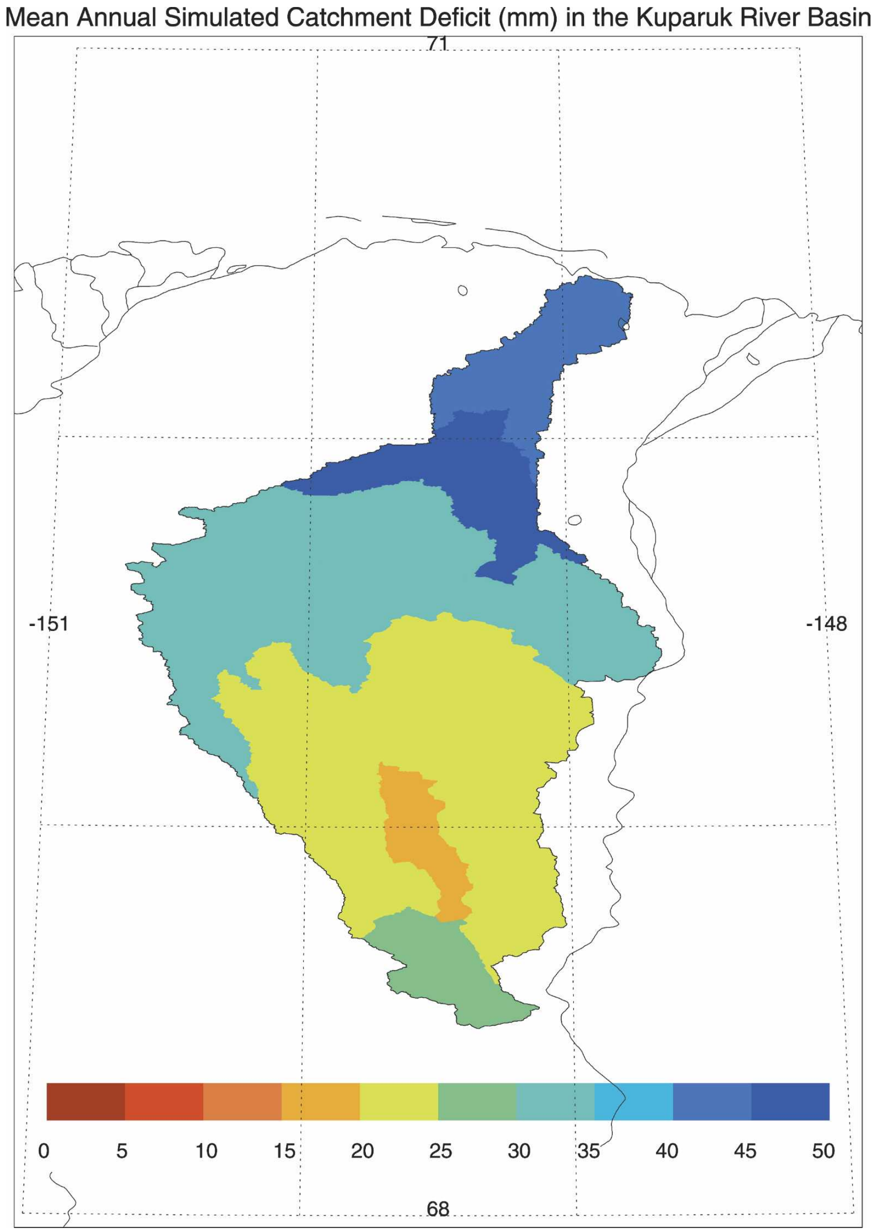

FIG. 9. The simulated mean annual catchment deficit (mm) in the Kuparuk River basin, 1991–2001.

those obtained by McNamara et al. (1998) who find that river runoff and evapotranspiration dispose 53% and 47% of the annual precipitation in the KRB, respectively.

Over the 11 yr of interest, considerable interannual variability exists in the air temperature and the water budget terms (Tables 3 and 5). Considering the uncertainty that remains in predicting the future response of Arctic watersheds to climate change, this prolonged study period allows a detailed investigation of the partitioning of the water budget for various climatic conditions. To this end, the annual ratios R/P and E/P based on the observations and simulations are plotted against the climate index defined in section 5. The objective here is to explore relationships and trends between the climatic state and the hydrologic response of the watershed.

We first examine the partitioning of the precipitation into river runoff and evapotranspiration based on observations. Here, the annual values of E are obtained as a residual in the water budget assuming no change in soil moisture, that is, $E = P - R$. Figure 11a provides a

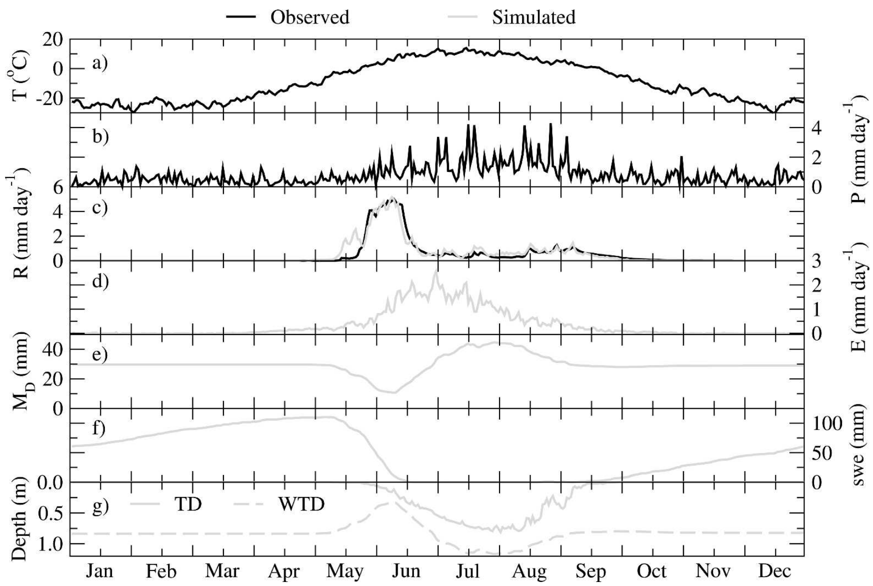

FIG. 10. The annual cycle of daily mean (a) observed air temperature (T), (b) observed precipitation rate (P), (c) observed and simulated runoff (R), (d) simulated evapotranspiration rate (E), (e) simulated catchment deficit (M_D), (f) simulated snow water equivalent (swe), and (g) simulated thaw depth (TD) and water table depth (WTD) for the Kuparuk River basin, 1991–2001.

comparison of the observed of R/P and E/P versus the climate index defined previously. Linear regressions performed on the data demonstrate that as conditions become relatively warm and dry, R/P increases whereas E/P decreases (Table 6). This suggests that river runoff intensifies during warm, dry years (relative to the precipitation input), whereas evapotranspiration does not. However, the regressions remain relatively weak since they do not pass the hypothesis of zero correlation at the $p < 0.1$ level (Table 6).

TABLE 5. Components of the water budget in the Kuparuk River basin, 1991–2001. The source term is precipitation (P) based on observations, and the sink terms are river runoff (R), evapotranspiration (E), and a change in soil moisture (ΔS), all based on the numerical simulations.

Year	P (mm)	R (mm)	E (mm)	ΔS (mm)	R/P	E/P	$\Delta S/P$
1991	328	204	127	0	0.62	0.39	0.00
1992	302	136	142	−6	0.45	0.47	−0.02
1993	281	161	125	16	0.57	0.44	0.06
1994	340	180	138	4	0.53	0.41	0.01
1995	271	223	96	−4	0.83	0.35	−0.01
1996	299	199	101	3	0.66	0.34	0.01
1997	318	201	110	9	0.63	0.36	0.02
1998	246	148	128	−18	0.60	0.55	−0.08
1999	336	157	144	11	0.47	0.45	0.03
2000	232	146	119	−6	0.63	0.54	−0.02
2001	265	122	123	1	0.46	0.48	0.01
Mean	292	169	127	1	0.60	0.41	0.01

Figure 11b depicts the same ratios as inferred from the numerical simulations versus the climate index. In this case, R/P and E/P both increase with decreasing values of the climate index, indicative of a more responsive watershed (relative to the precipitation input) during relatively warm and dry conditions (see further discussion in section 7b). The slope of the linear regressions for the observed and simulated ratios of R/P are nearly equal ($\approx -2.6\%$ per unit of the climate index). This indicates that the CLSM is capturing the observed interannual variability in river runoff for this watershed. However, the slopes of the linear regressions for the observed and simulated E/P ratios are of opposite sign and are once again relatively weak (Table 6). The consideration of soil moisture as a dynamic water reservoir by the CLSM leads to the discrepancies between the observed and simulated ratios of E/P.

From the linear regressions performed on the simulation results, the sum of R/P and E/P equals unity when the climate index is 0.51 (Fig. 11b). Its proximity to zero implies that the current state of the water budget is in equilibrium with the climate of the KRB to moderate long-term variations in soil moisture conditions. If the climate index during one year diminishes below 0.51, a drying out of soils occurs as both sinks in the water budget combine to surpass the precipitation input. On the other hand, when the climate index is above 0.51, precipitation exceeds river runoff and evapotranspiration, leading to a net gain in soil mois-

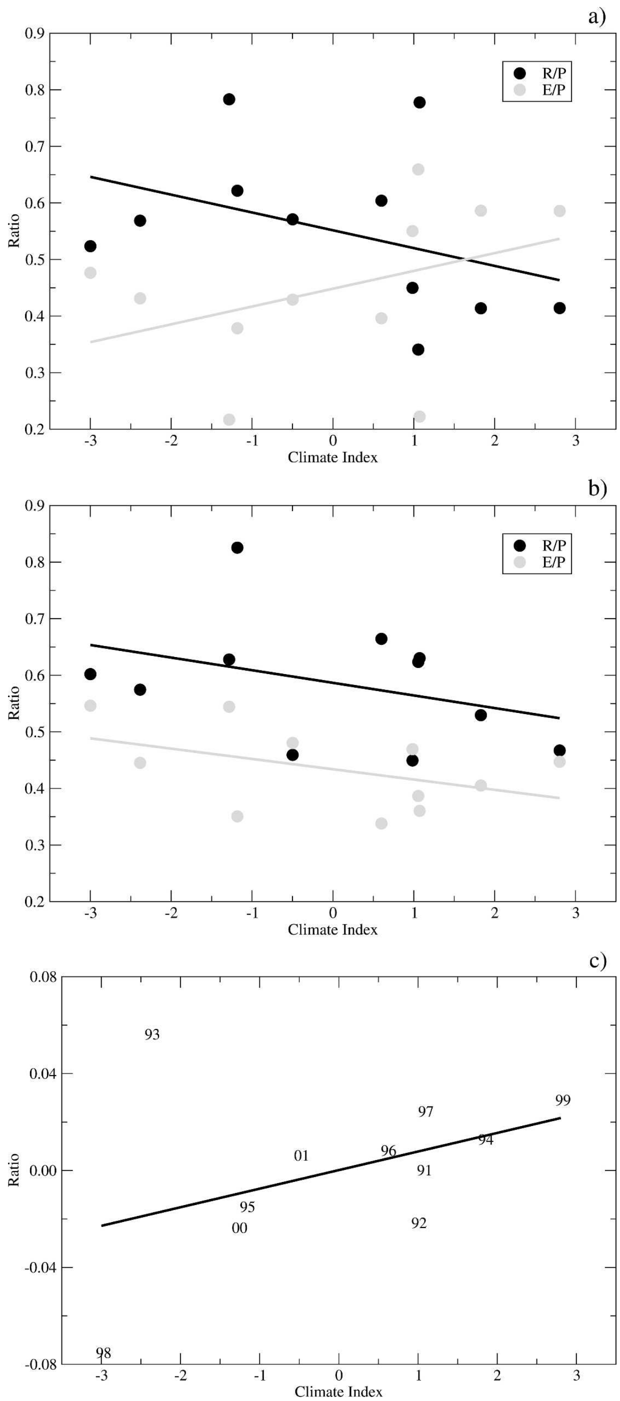

Fig. 11. The annual ratios of (a) observed R/P and E/P, (b) simulated R/P and E/P, and (c) simulated $\Delta S/P$ vs the climate index for the Kuparuk River basin, 1991–2001. Statistics for the linear regressions (thick lines) are given in Table 6, and the last two digits of each year are indicated for each data point in (c).

ture. Figure 11c confirms this tendency in the numerical simulations. The relation between the climate index and the amount of water stored in soils shows a positive correlation of 0.40 (see Table 6).

Table 6. The correlation coefficients (R), slopes (m), and probability values (p) for the linear regressions of climate index values vs the observed and simulated ratios of R/P, E/P, and $\Delta S/P$ (see Fig. 11).

	Observed		Simulated		
Regression statistic	R/P	E/P	R/P	E/P	$\Delta S/P$
R	−0.40	0.40	−0.37	−0.45	0.40
m	−0.031	0.031	−0.022	−0.018	0.008
p	0.23	0.23	0.27	0.16	0.22

b. *Seasonal variability*

For 1993, however, the CLSM shows an increase in soil moisture during a warm, dry year. This unexpected result can be explained by a seasonal evaluation of the water budget. Figure 12 illustrates the relationship between the seasonal values of observed precipitation and air temperature over the KRB during the period 1991–2001. Highlighted on this plot are the results for two warm, dry years (1993 and 1998) and one cool, wet year (1999). In 1993, the greatest positive air temperature departures from the mean occur during fall, winter, and spring, whereas the greatest negative precipitation departure from the mean occurs during summer. These large deviations from the average air temperature and precipitation lead to a large negative climate index that year. However, late summer and fall are marked by low evapotranspiration (not shown) and above-average precipitation. These factors generate soil moisture recharge just before freeze-up that explains the atypical response of the watershed in 1993. Excluding the results for 1993 improves the correlation coefficient between the climate index and the change in soil moisture from 0.40 to 0.85, yielding a relation that is significant at the $p < 0.002$ level.

The seasonal variability in air temperature and precipitation also explains the simulated tendencies of R/P and E/P. During warm, dry years, these ratios increase since precipitation decreases during summer when evapotranspiration rates are most intense; that is, E varies little relative to the decrease in precipitation, yielding the higher E/P ratio. Cool, wet years however are marked by lower values of R/P and E/P since the summertime precipitation increase surpasses both those in river runoff and evapotranspiration.

Although the climate index defined in section 4a provides a convenient measure of the annual state of the climate, Fig. 12 demonstrates that it may mask some strong seasonal variations in air temperature and precipitation. Indeed, the annual climate index values are dominated by departures from the mean seasonal air temperatures during fall, winter, and spring in addition to departures from the average seasonal precipitation

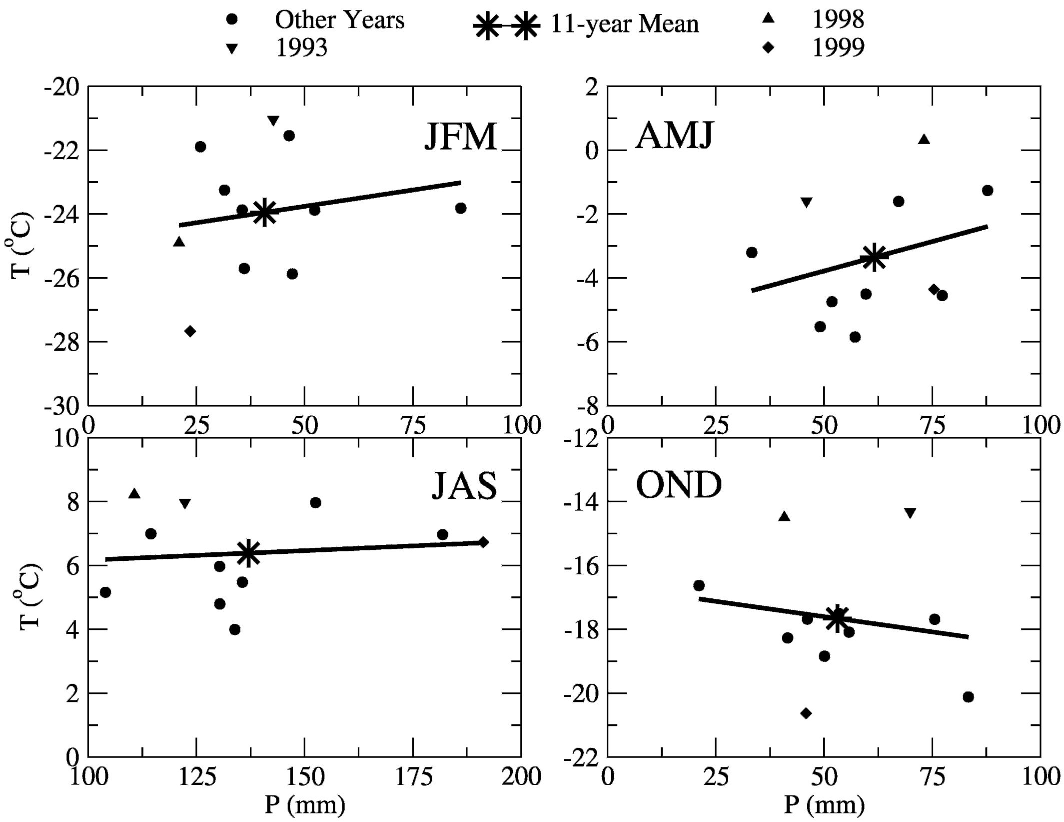

FIG. 12. The relationship between the seasonal values of observed precipitation (P) and surface air temperature (T) in the KRB, 1991–2001. Statistics for the linear regressions (black lines) are given in Table 7.

during summer. The relatively warm, dry years of 1993 and 1998 arise from warmer-than-average cold-season air temperatures and a dry warm season. On the other hand, the relatively cool, wet year of 1999 arises from cooler-than-average wintertime air temperatures and wetter-than-average summertime conditions. Table 6 provides the statistical evidence that T varies most during the cool season and P varies most during the warm season. It is this seasonal variability that dominates the annual climate index values. Although a positive relationship between the climate index and changes in soil moisture is found in Fig. 11c, there are years such as 1993 when this association breaks down owing to the precise timing of the precipitation and air temperature departures. Figure 12 also demonstrates the poor relationship that exists between seasonal values of precipitation and air temperature since all four linear regressions fail to pass the hypothesis of zero correlation at the $p < 0.1$ level (Table 7).

c. Potential future state of the KRB water budget

The strong seasonal variability in air temperature and precipitation has significant implications for the future state of the KRB's water budget. GCM simulations suggest that future warming in the Arctic will occur predominantly during winter (e.g., Holland and Bitz 2003). If this warming accompanies greater snowfall, then the additional precipitation would tend to run off quickly during spring when soils are frozen. In this case, the watershed would respond as in 1998 with a decrease

TABLE 7. Values of the seasonal mean precipitation ($\overline{P}$) and air temperature ($\overline{T}$), the seasonal standard deviation of precipitation (s_P) and air temperature (s_T), and the correlation coefficients (R), slopes (m), and probability values (p) of the linear regressions between the seasonal values of P and T, 1991–2001 (see Fig. 12). Mean or total annual values are also provided. JFM: Jan–Feb–Mar; AMJ: Apr–May–Jun; JAS: Jul–Aug–Sep; OND: Oct–Nov–Dec.

Variable	JFM	AMJ	JAS	OND	Year
$\overline{P}$ (mm)	40.8	61.6	137.0	53.1	292.5
$\overline{T}$ (°C)	−24.0	−3.4	6.4	−17.7	−9.6
s_P (mm)	17.3	15.4	26.6	16.9	34.9
s_T (°C)	2.0	2.0	1.4	2.0	1.2
R	0.19	0.30	0.12	−0.17	−0.49
m	0.021	0.037	0.006	−0.019	−0.016
p	0.59	0.38	0.73	0.61	0.13

in soil moisture. However, if the positive precipitation anomalies occur during summer and fall before freeze-up of the active layer, then soil moisture will increase on average. Clearly, the exact timing of the temperature and precipitation increases in a changing Arctic climate will determine the future state of the KRB's water budget.

8. Summary and future work

This study provides the first long-term analysis of the observed and simulated water budgets for the Kuparuk River basin (KRB) of Alaska. Numerical simulations of hydrologic processes using the Catchment-based Land Surface Model (CLSM) for the period 1991–2001 provide the partitioning of the observed precipitation input (292 mm yr^{-1}) onto the KRB into river discharge (169 mm yr^{-1}), evapotranspiration (127 mm yr^{-1}), and an increase in soil moisture (1 mm yr^{-1}). Discharge attains its annual peak during snowmelt and disposes 58% of the annual precipitation. Evapotranspiration contributes another 43% to the water budget and is mainly associated with warm summertime conditions and a snow-free surface. Combined, surface- and blowing-snow sublimation contribute only 5% of the total annual evaporative fluxes. Soil moisture recharge is associated with snowmelt during spring, and rainfall during late summer and early fall, whereas soil drying accompanies high evapotranspiration rates during summer. An analysis of interannual variability in the simulated water budget shows that warm, dry years favor a relatively more intense response of river discharge and of evapotranspiration to the precipitation input, whereas cool, wet years tend to augment soil moisture.

Although this study provides a better understanding of the KRB's water budget, several topics remain priorities for future work. First, the numerical simulations of soil moisture need to be validated with observational data. This step is crucial since most ecological models, such as the General Ecology Model (GEM; Rastetter et al. 1991) or the Soil–Plant–Atmosphere (SPA) model (Williams et al. 1996, 2001) all require the correct soil moisture distribution for accurate simulations of the net primary production and other vegetation parameters at fine spatial scales (e.g., Engel et al. 2002). Since the CLSM tracks both the soil thermal and moisture regimes, its coupling to an ecological model will improve the spatial and temporal representation of subsurface conditions and aid in the forcing of plant growth and soil decay models on the North Slope of Alaska. Second, the applicability of the climate index to study the partitioning of the water budget terms must be explored using long-term meteorological datasets and numerical simulations. The climate index thus may provide a useful measure of the interannual variability in air temperature and precipitation to study the role of large-scale atmospheric anomalies on the water budget of pan-Arctic river basins (e.g., Déry and Wood 2004, 2005). These steps will further our knowledge of the processes governing the water budget of the KRB and will help refine predictions of its future state.

Acknowledgments. This project was funded through support by National Science Foundation Grant OPP-0082361 (E. F. Wood). We acknowledge that funding for M. Stieglitz is provided from National Science Foundation (NSF) grants from the Office of Polar Programs (OPP-002369), from the division of Environmental Biology (Arctic LTER Project), and from an NSF Cooperative Agreement (OPP-0002239), as well as the National Aeronautics and Space Administration's (NASA's) Seasonal-to-Interannual Prediction Project at Goddard Space Flight Center, NASA's Global Modeling and Analysis Program under RTOP 622-24-47, and the NSF Biocomplexity Award ATM 0221835. We thank R. D. Koster, S. Mahanama, R. Reichle, M. J. Suarez (NASA GSFC), and J. W. Walker (University of Melbourne) for technical support with the CLSM and three anonymous referees for their useful comments. We are grateful to D. L. Kane and L. D. Hinzman (University of Alaska Fairbanks) for access to their comprehensive North Slope observational database, J. Hobbie, G. R. Shaver, and J. M. Laundre (MBL, Woods Hole) for access to the Arctic LTER database, D. F. Meyer (USGS, Alaska Science Center) for insights on the accuracy of streamflow data for the Kuparuk River, and M. Nolan (University of Alaska Fairbanks) for supplying the digital elevation model.

REFERENCES

Barber, V. A., G. P. Juday, and B. P. Finney, 2000: Reduced growth of Alaskan white spruce in the twentieth century from temperature-induced drought stress. *Nature,* **405,** 668–673.

Beven, K. J., 1997: TOPMODEL: A critique. *Hydrol. Processes,* **11,** 1069–1085.

——, and M. J. Kirkby, 1979: A physically-based variable contributing area model of basin hydrology. *Hydrol. Sci. Bull.,* **24,** 43–69.

Bowling, L. C., D. L. Kane, R. E. Gieck, L. D. Hinzman, and D. P. Lettenmaier, 2003: The role of surface storage in a low-gradient Arctic watershed. *Water Resour. Res.,* **39,** 1087, doi:10.1029/2002WR001466.

——, J. W. Pomeroy, and D. P. Lettenmaier, 2004: Parameterization of blowing-snow sublimation in a macroscale hydrology model. *J. Hydrometeor.,* **5,** 745–762.

Chapman, W. L., and J. E. Walsh, 1993: Recent variations in sea ice and air temperature in high latitudes. *Bull. Amer. Meteor. Soc.,* **74,** 33–47.

Déry, S. J., and M. K. Yau, 1999: A climatology of adverse winter-type weather events. *J. Geophys. Res.,* **104,** 16 657–16 672.

——, and ——, 2001a: Simulation of an Arctic ground blizzard using a coupled blowing snow–atmosphere model. *J. Hydrometeor.,* **2,** 579–598.

——, and ——, 2001b: Simulation of blowing snow in the Canadian Arctic using a double-moment model. *Bound.-Layer Meteor.,* **99,** 297–316.

——, and ——, 2002: Large-scale mass balance effects of blowing snow and surface sublimation. *J. Geophys. Res.,* **107,** 4679, doi:10.1029/2001JD001251.

——, and E. F. Wood, 2004: Teleconnection between the Arctic Oscillation and Hudson Bay river discharge. *Geophys. Res. Lett.,* **31,** L18205, doi:10.1029/2004GL020729.

——, and ——, 2005: Decreasing river discharge in northern Canada. *Geophys. Res. Lett.,* **32,** L10401, doi:10.1029/2005GL022845.

——, P. A. Taylor, and J. Xiao, 1998: The thermodynamic effects of sublimating, blowing snow in the atmospheric boundary layer. *Bound.-Layer Meteor.,* **89,** 251–283.

——, W. T. Crow, M. Stieglitz, and E. F. Wood, 2004: Modeling snow-cover heterogeneity over complex Arctic terrain for regional and global climate models. *J. Hydrometeor.,* **5,** 33–48.

——, V. V. Salomonson, M. Stieglitz, D. K. Hall, and I. Appel, 2005: An approach to using snow areal depletion curves inferred from MODIS and its application to land surface modelling in Alaska. *Hydrol. Processes,* **19,** doi:10.1002/hyp.5784.

Ducharne, A., R. D. Koster, M. J. Suarez, M. Stieglitz, and P. Kumar, 2000: A catchment-based approach to modeling land surface processes in a general circulation model. 2. Parameter estimation and model demonstration. *J. Geophys. Res.,* **105,** 24 823–24 838.

Engel, V. C., M. Stieglitz, M. Williams, and K. L. Griffin, 2002: Forest canopy hydraulic properties and catchment water balance: Observations and modeling. *Ecol. Modell.,* **154,** 263–288.

French, H. M., 1993: Cold-climate processes and landforms. *Canada's Cold Environments,* H. M. French and O. Slaymaker, Eds., McGill Queen's Press, 143–167.

Hinzman, L. D., and D. L. Kane, 1991: Snow hydrology of a headwater Arctic basin. 2. Conceptual analysis and computer modeling. *Water Resour. Res.,* **27,** 1111–1121.

——, and ——, 1992: Potential response of an Arctic watershed during a period of global warming. *J. Geophys. Res.,* **97,** 2811–2820.

——, ——, R. E. Gieck, and K. R. Everett, 1991: Hydrologic and thermal-properties of the active layer in the Alaskan Arctic. *Cold Reg. Sci. Technol.,* **19,** 95–110.

——, ——, C. S. Benson, and K. R. Everett, 1996: Energy balance and hydrological processes in an Arctic watershed. *Landscape Function and Disturbance in Arctic Tundra,* Vol. 120, J. F. Reynolds and J. D. Tenhunen, Eds., Ecological Studies, Springer-Verlag, 131–154.

——, D. J. Goering, and D. L. Kane, 1998: A distributed thermal model for calculating soil temperature profiles and depth of thaw in permafrost regions. *J. Geophys. Res.,* **103,** 28 975–28 991.

Holland, M. M., and C. M. Bitz, 2003: Polar amplification of climate change in coupled models. *Climate Dyn.,* **21,** 221–232.

Jones, H. G., 1992: *Plants and Microclimate: A Quantitative Approach to Environmental Plant Physiology.* 2d ed. Cambridge University Press, 428 pp.

Jordan, R., 1991: A one-dimensional temperature model for a snow cover. U.S. Army Corps of Engineers, Cold Regions Research and Engineering Laboratory, Special Rep. 91–16, 49 pp.

Kane, D. L., and L. D. Hinzman, cited 2003: Climate data from the North Slope Hydrology Research project. University of Alaska Fairbanks, Water and Environmental Research Center, Fairbanks, AK. [Available online at http://www.uaf.edu/water/projects/NorthSlope/.]

——, R. E. Gieck, and L. D. Hinzman, 1990: Evapotranspiration from a small Alaskan Arctic watershed. *Nord. Hydrol.,* **21,** 253–272.

——, L. D. Hinzman, C. S. Benson, and G. E. Liston, 1991a: Snow hydrology of a headwater Arctic basin. 1. Physical measurements and process studies. *Water Resour. Res.,* **27,** 1099–1109.

——, ——, and J. P. Zarling, 1991b: Thermal response of the active layer to climatic warming in a permafrost environment. *Cold Reg. Sci. Technol.,* **19,** 111–122.

——, ——, J. P. McNamara, Z. Zhang, and C. S. Benson, 2000: An overview of a nested watershed study in Arctic Alaska. *Nord. Hydrol.,* **31,** 245–266.

——, R. E. Gieck Jr., L. D. Hinzman, and E. K. Lilly, 2002: Meteorologic and Hydrologic Data Sets for the North Slope of Alaska along the Kuparuk River Watershed 1985–1997. Tech. Rep., Water Research Center, Institute of Northern Engineering, University of Alaska Fairbanks, 52 pp.

König, M., and M. Sturm, 1998: Mapping snow distribution in the Alaskan Arctic using aerial photography and topographic relationships. *Water Resour. Res.,* **34,** 3471–3483.

Koster, R. D., and M. J. Suarez, 1996: Energy and Water Balance Calculations in the Mosaic LSM. NASA Tech. Memo. 104606, Vol. 9, 59 pp.

——, ——, A. Ducharne, M. Stieglitz, and P. Kumar, 2000: A catchment-based approach to modeling land surface processes in a general circulation model. 1. Model structure. *J. Geophys. Res.,* **105,** 24 809–24 822.

Liston, G. E., and M. Sturm, 1998: A snow-transport model for complex terrain. *J. Glaciol.,* **44,** 498–516.

——, and ——, 2002: Winter precipitation patterns in Arctic Alaska determined from a blowing snow model and snow-depth observations. *J. Hydrometeor.,* **3,** 646–659.

Luce, C. H., D. G. Tarboton, and K. R. Cooley, 1998: The influence of the spatial distribution of snow on basin-averaged snowmelt. *Hydrol. Processes,* **12,** 1671–1683.

Lynch-Stieglitz, M., 1994: The development and validation of a simple snow model for the GISS GCM. *J. Climate,* **7,** 1842–1855.

McNamara, J. P., D. L. Kane, and L. D. Hinzman, 1997: Hydrograph separations in an Arctic watershed using mixing model and graphical techniques. *Water Resour. Res.,* **33,** 1707–1719.

——, ——, and ——, 1998: An analysis of streamflow hydrology in the Kuparuk River Basin, Arctic Alaska: A nested watershed approach. *J. Hydrol.,* **206,** 39–57.

Mendez, J., L. D. Hinzman, and D. L. Kane, 1998: Evapotranspiration from a wetland complex on the Arctic Coastal Plain of Alaska. *Nord. Hydrol.,* **29,** 303–330.

Miller, J. R., G. L. Russell, and G. Caliri, 1994: Continental-scale river flow in climate models. *J. Climate,* **7,** 914–928.

Nolan, M., 2003: Distribution of a Star3i DEM of the Kuparuk

River watershed. Joint Office of Scientific Support, Boulder, CO, CD-ROM.

Oke, T. R., 1987: *Boundary Layer Climates.* 2d ed. Methuen, 435 pp.

Olsson, P. Q., M. Sturm, C. H. Racine, V. Romanovsky, and G. E. Liston, 2003: Five stages of the Alaskan Arctic cold season with ecosystem implications. *Arct. Antarct. Alp. Res.,* **35,** 74–81.

Ostendorf, B., P. Quinn, K. Beven, and J. D. Tenhunen, 1996: Hydrological controls on ecosystem gas exchange in an arctic landscape. *Landscape Function and Disturbance in Arctic Tundra,* Vol. 120, J. F. Reynolds and J. D. Tenhunen, Eds., Ecological Studies, Springer-Verlag, 369–386.

Osterkamp, T. E., and M. W. Payne, 1981: Estimates of permafrost thickness from well logs in northern Alaska. *Cold Reg. Sci. Technol.,* **5,** 13–27.

——, and V. E. Romanovsky, 1996: Characteristics of changing permafrost temperatures in the Alaskan Arctic, U.S.A. *Arct. Alp. Res.,* **28,** 267–273.

——, and ——, 1997: Freezing of the active layer on the Coastal Plain of the Alaskan Arctic. *Perm. Perigl. Proc.,* **8,** 23–44.

Peterson, B. J., R. M. Holmes, J. W. McClelland, C. J. Vörösmarty, R. B. Lammers, A. I. Shiklomanov, I. A. Shiklomanov, and S. Rahmstorf, 2002: Increasing river discharge to the Arctic Ocean. *Science,* **298,** 2171–2173.

Quinn, P. F., B. Ostendorf, K. Beven, and J. D. Tenhunen, 1998: Spatial and temporal predictions of soil moisture patterns and evaporative losses using TOPMODEL and the GASFLUX model for an Alaskan catchment. *Hydrol. Earth Syst. Sci.,* **2,** 51–64.

Rastetter, E. B., M. G. Ryan, G. R. Shaver, J. M. Melillo, K. J. Nadelhoffer, J. E. Hobbie, and J. D. Aber, 1991: A general biogeochemical model describing the responses of the C-cycle and N-cycle in terrestrial ecosystems to changes in CO2, climate, and N-deposition. *Tree Physiol.,* **9,** 101–126.

Romanovsky, V. E., and T. E. Osterkamp, 1997: Thawing of the active layer on the Coastal Plain of the Alaskan Arctic. *Perm. Perigl. Proc.,* **8,** 1–22.

Serreze, M. C., and Coauthors, 2000: Observational evidence of recent change in the northern high-latitude environment. *Climatic Change,* **46,** 159–207.

——, D. H. Bromwich, M. P. Clark, A. J. Etringer, T. Zhang, and R. Lammers, 2003: Large-scale hydro-climatology of the terrestrial Arctic drainage system. *J. Geophys. Res.,* **108,** 8160, doi:10.1029/2001JD000919.

Shaman, J., M. Stieglitz, V. Engel, R. Koster, and C. Stark, 2002: Representation of subsurface storm flow and a more responsive water table in a TOPMODEL-based hydrology model. *Water Resour. Res.,* **38,** 1156, doi:10.1029/2001WR000636.

Shiklomanov, N. I., and F. E. Nelson, 1999: Analytic representation of the active layer thickness field, Kuparuk River Basin, Alaska. *Ecol. Modell.,* **123,** 105–125.

——, and ——, 2002: Active-layer mapping at regional scales: A 13-year spatial time series for the Kuparuk Region, North-Central Alaska. *Perm. Perigl. Proc.,* **13,** 219–230.

Sivapalan, M., K. Beven, and E. F. Wood, 1987: On hydrologic similarity. 2. A scaled model of storm runoff production. *Water Resour. Res.,* **23,** 2266–2278.

Stieglitz, M., J. Hobbie, A. Giblin, and G. Kling, 1999: Hydrologic modeling of an arctic tundra watershed: Toward pan-Arctic predictions. *J. Geophys. Res.,* **104,** 27 507–27 518.

——, A. Giblin, J. Hobbie, M. Williams, and G. Kling, 2000: Simulating the effects of climate change and climate variability on carbon dynamics in Arctic tundra. *Global Biogeochem. Cycles,* **14,** 1123–1136.

——, A. Ducharne, R. Koster, and M. Suarez, 2001: The impact of detailed snow physics on the simulation of snow cover and subsurface thermodynamics at continental scales. *J. Hydrometeor.,* **2,** 228–242.

——, S. J. Déry, V. E. Romanovsky, and T. E. Osterkamp, 2003a: The role of snow cover in the warming of Arctic permafrost. *Geophys. Res. Lett.,* **30,** 1721, doi:10.1029/2003GL017337.

——, J. Shaman, J. McNamara, G. W. Kling, V. Engel, and J. Shanley, 2003b: An approach to understanding hydrologic connectivity on the hillslope and the implications for nutrient transport. *Global Biogeochem. Cycles,* **17,** 1105, doi:10.1029/2003GB002041.

Taras, B., M. Sturm, and G. E. Liston, 2002: Snow-ground interface temperatures in the Kuparuk River Basin, Arctic Alaska: Measurements and model. *J. Hydrometeor.,* **3,** 377–394.

Walker, D. A., and M. D. Walker, 1996: Terrain and vegetation of the Imnavait Creek watershed. *Landscape Function and Disturbance in Arctic Tundra,* J. F. Reynolds and J. D. Tenhunen, Eds., Ecological Studies, Vol. 120, Springer-Verlag, 73–108.

Walsh, J. E., 2000: Global atmospheric circulation patterns and relationships to Arctic freshwater fluxes. *The Freshwater Budget of the Arctic Ocean,* E. L. Lewis, Ed., Kluwer Academic, 21–44.

Williams, M., and Coauthors, 1996: Modelling the soil–plant–atmosphere continuum in a *Quercus-Acer* stand at Harvard Forest: The regulation of stomatal conductance by light, nitrogen, and soil/plant hydraulic properties. *Plant Cell Environ.,* **19,** 911–927.

——, B. E. Law, P. M. Anthoni, and M. H. Unsworth, 2001: Use of a simulation model and ecosystem flux data to examine carbon-water interactions in ponderosa pine. *Tree Physiol.,* **21,** 287–298.

Xiao, J., R. Bintanja, S. J. Déry, G. W. Mann, and P. A. Taylor, 2000: An intercomparison among four models of blowing snow. *Bound.-Layer Meteor.,* **97,** 109–135.

Yang, D., and Coauthors, 2000: An evaluation of the Wyoming gauge system for snowfall measurement. *Water Resour. Res.,* **36,** 2665–2677.

Zhang, T., T. E. Osterkamp, and K. Stamnes, 1996: Some characteristics of the climate in Northern Alaska, U.S.A. *Arct. Alp. Res.,* **28,** 509–518.

——, ——, and ——, 1997: Effects of climate on the active layer and permafrost on the North Slope of Alaska, U.S.A. *Perm. Perigl. Proc.,* **8,** 45–67.

Zhang, Z., D. L. Kane, and L. D. Hinzman, 2000: Development and application of a spatially-distributed Arctic hydrological and thermal process model (ARHYTHM). *Hydrol. Processes,* **14,** 1017–1044.